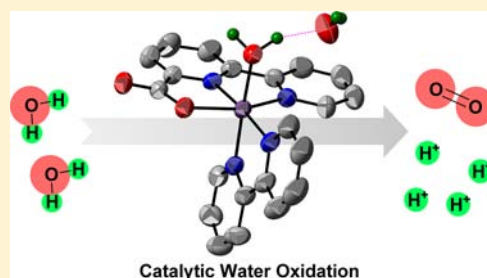


## Catalytic Water Oxidation by Mononuclear Ru Complexes with an Anionic Ancillary Ligand

Lianpeng Tong,<sup>†</sup> A. Ken Inge,<sup>‡</sup> Lele Duan,<sup>†</sup> Lei Wang,<sup>†</sup> Xiaodong Zou,<sup>‡</sup> and Licheng Sun<sup>\*,†,§</sup><sup>†</sup>Department of Chemistry, School of Chemical Science and Engineering, KTH Royal Institute of Technology, SE-100 44 Stockholm, Sweden<sup>‡</sup>Berzelii Centre EXSELENT on Porous Materials and Inorganic and Structural Chemistry, Department of Materials and Environmental Chemistry, Stockholm University, SE-106 91 Stockholm, Sweden<sup>§</sup>DUT-KTH Joint Education and Research Center on Molecular Devices, State Key Laboratory of Fine Chemicals, Dalian University of Technology (DUT), 116012, Dalian, China

## Supporting Information

**ABSTRACT:** Mononuclear Ru-based water oxidation catalysts containing anionic ancillary ligands have shown promising catalytic efficiency and intriguing properties. However, their insolubility in water restricts a detailed mechanism investigation. In order to overcome this disadvantage, complexes  $[\text{Ru}^{\text{II}}(\text{bpc})(\text{bpy})\text{OH}_2]^+$  ( $1^+$ , bpc = 2,2'-bipyridine-6-carboxylate, bpy = 2,2'-bipyridine) and  $[\text{Ru}^{\text{II}}(\text{bpc})(\text{pic})_3]^+$  ( $2^+$ , pic = 4-picoline) were prepared and fully characterized, which features an anionic tridentate ligand and has enough solubility for spectroscopic study in water. Using  $\text{Ce}^{\text{IV}}$  as an electron acceptor, both complexes are able to catalyze  $\text{O}_2$ -evolving reaction with an impressive rate constant. On the basis of the electrochemical and kinetic studies, a water nucleophilic attack pathway was proposed as the dominant catalytic cycle of the catalytic water oxidation by  $1^+$ , within which several intermediates were detected by MS. Meanwhile, an auxiliary pathway that is related to the concentration of  $\text{Ce}^{\text{IV}}$  was also revealed. The effect of anionic ligand regarding catalytic water oxidation was discussed explicitly in comparison with previously reported mononuclear Ru catalysts carrying neutral tridentate ligands, for example, 2,2':6',2''-terpyridine (tpy). When  $2^+$  was oxidized to the trivalent state, one of its picoline ligands dissociated from the Ru center. The rate constant of picoline dissociation was evaluated from time-resolved UV-vis spectra.



## INTRODUCTION

Oxidation of water to molecular oxygen ( $2\text{H}_2\text{O} \rightarrow \text{O}_2 + 4\text{H}^+ + 4\text{e}^-$ ) is a vital reaction in either naturally occurring or an envisaged artificial photosynthesis that converts solar energy to chemical energy.<sup>1,2</sup> In the biological world, water oxidation is catalyzed by the oxygen-evolving complex (OEC) of Photosystem II (PSII).<sup>3</sup> There has been a long-standing effort for chemists to develop practically applicable catalysts that can duplicate the function of OEC in the context of solar energy utilization.<sup>4,5</sup> Over the past few years, emergence of single-site Ru complexes that are capable of catalyzing  $\text{O}_2$  evolution from water has shed new light in this field.<sup>6,7</sup> Their well-defined chemical properties and tailorable ligands allow for profound mechanism investigation and feasibility of systematic structure design. Furthermore, research on Ru-based molecular water oxidation catalysts (WOC) has accumulated valuable experience for development of first-row transition-metal-based WOCs.<sup>8</sup>

Most of the reported mononuclear Ru WOCs carry a polypyridyl ancillary ligand, and their coordinative matrices can be roughly categorized into the following motives:  $[\text{Ru}(\text{N}_3)(\text{N}_2)\text{L}]$ ,  $[\text{Ru}(\text{N}_3)(\text{N}_1)_2\text{L}]$ , and  $[\text{Ru}(\text{N}_4)(\text{N}_1)_2]$  ( $\text{N}_n = n$ -dentate nitrogen-heterocyclic ligand and  $\text{L} =$  monodentate non-nitrogen ligand, water or halogen typically).<sup>9–18</sup> Mechanistic

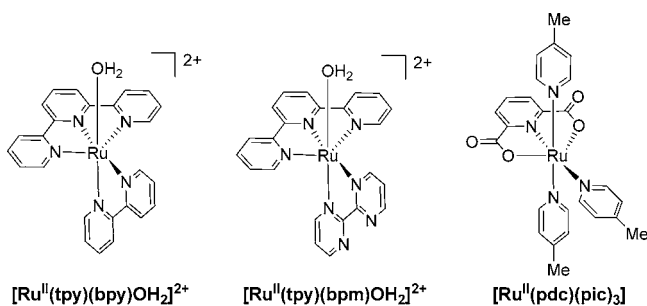
studies based on these competent Ru WOCs have established the following fundamental facts: (i) the catalytic cycle of water oxidation is an intricate process that contains multiple steps; (ii) high-valent ruthenium intermediates, such as  $[\text{Ru}^{\text{IV}}=\text{O}]$  and  $[\text{Ru}^{\text{V}}=\text{O}]$ , are involved in the cycle; and (iii) the critical step of O–O bond formation can undergo diverse pathways that are relevant to both structures of WOCs and conditions of catalytic reaction.<sup>15,19–23</sup> Experimental results also demonstrated that properties of ancillary ligands including electronic parameters, flexibility, and orientation influence the activity of mononuclear Ru WOCs significantly.<sup>10,15,16,24</sup> However, there is not enough proof yet to elucidate correlations between the performance, mechanism, and ligand environments of WOCs.

Our research group has synthesized and characterized several series of  $\text{Ru}^{\text{II}}$  molecular WOCs featuring anionic donors (carboxylic and phenonate group specifically) as ancillary ligands.<sup>25–30</sup> Recent examples of our work are  $[\text{Ru}^{\text{II}}(\text{pdc})(\text{pic})_3]$  and  $[\text{Ru}^{\text{II}}(\text{hqc})(\text{pic})_3]$  (Scheme 1,  $\text{H}_2\text{pdc} =$  2,6-pyridinedicarboxylic acid,  $\text{H}_2\text{hqc} =$  8-hydroxyquinoline-2-carboxylic acid, and  $\text{pic} =$  4-picoline), upon which a combination of experimental and theoretical investigations

Received: November 8, 2012

Published: February 14, 2013

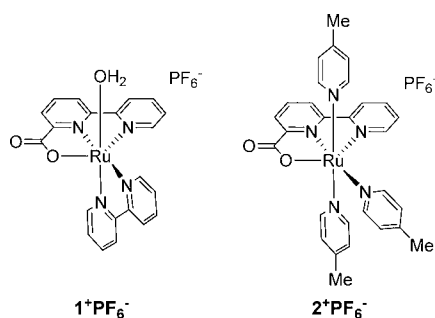
**Scheme 1. Structures of  $[\text{Ru}^{\text{II}}(\text{tpy})(\text{bpy})\text{OH}_2]^{2+}$ ,  $[\text{Ru}^{\text{II}}(\text{tpy})(\text{bpm})\text{OH}_2]^{2+}$ , and  $[\text{Ru}^{\text{II}}(\text{pdc})(\text{pic})_3]$  Reported Previously**



were carried out.<sup>31</sup> It has been revealed that, in comparison with the neutral tridentate 2,2':6',2''-terpyridine (tpy) ligand, tridentate anionic pdc and hqc ligands facilitate electron transfer (ET) from Ru complexes to the oxidant (tetravalent cerium typically) and labilize the Ru–N(picoline) bond. Moreover, both  $[\text{Ru}^{\text{II}}(\text{pdc})(\text{pic})_3]$  and  $[\text{Ru}^{\text{II}}(\text{hqc})(\text{pic})_3]$  are able to catalyze the water oxidation reaction efficiently (turnover frequency = 0.23 and 0.32  $\text{s}^{-1}$ , respectively), in which the anionic dative ligands are purported to play an essential role. However, an explicit mechanism study based on these two candidates was not achieved because their negatively charged coordination sphere offsets the positive charge of the Ru core, and as a result complexes  $[\text{Ru}^{\text{II}}(\text{pdc})(\text{pic})_3]$  and  $[\text{Ru}^{\text{II}}(\text{hqc})(\text{pic})_3]$  are neutral in charge and insoluble in water.

Aiming to evaluate the contribution of anionic ligands to the catalytic performance of WOCs, we elaborately designed and prepared two Ru complexes  $[\text{Ru}^{\text{II}}(\text{bpc})(\text{bpy})\text{OH}_2]^+$  ( $1^+$ ) and  $[\text{Ru}^{\text{II}}(\text{bpc})(\text{pic})_3]^+$  ( $2^+$ ) (Scheme 2, Hbpc = 2,2'-bipyridine-6-

**Scheme 2. Structures of  $[\text{Ru}^{\text{II}}(\text{bpc})(\text{bpy})\text{OH}_2]^+\text{PF}_6^-$  ( $1^+\text{PF}_6^-$ ) and  $[\text{Ru}^{\text{II}}(\text{bpc})(\text{pic})_3]^+\text{PF}_6^-$  ( $2^+\text{PF}_6^-$ ) Investigated in This Work**



carboxylic acid, bpy = 2,2'-bipyridine). Introduction of the tridentate monoanionic ligand, bpc, keeps certain solubility of  $1^+$  and  $2^+$  in water and thus allows spectroscopic studies in aqueous solution without any organic cosolvents (no interference from chelating organic solvents). In the current study, we examined the properties of these two complexes and discussed their catalytic pathway based on collective observations from electrochemistry, UV–vis, stopped-flow, ESI-MS, and  $\text{O}_2$ -evolving experiments. The goal is to offer specific evidence about how an anionic group, rather than neutral ligands, enhances the catalytic activity of Ru WOCs. In such a way, better understanding of the structure–mechanism correlation was achieved in terms of water oxidation mediated by molecular WOCs.

The coordination motif of  $1^+$  is very similar to that of  $[\text{Ru}^{\text{II}}(\text{tpy})(\text{bpy})\text{OH}_2]^{2+}$  and  $[\text{Ru}^{\text{II}}(\text{tpy})(\text{bpm})\text{OH}_2]^{2+}$  (Scheme 1, bpm = 2,2'-bipyrimidine), which are prototypes of  $[\text{Ru}(\text{N}_3)(\text{N}_2)\text{L}]$  WOCs aforementioned. The catalytic kinetics and mechanisms of  $[\text{Ru}^{\text{II}}(\text{tpy})(\text{bpm})\text{OH}_2]^{2+}$  were initially examined by Meyer's group.<sup>20,21</sup> The catalytic behavior of  $[\text{Ru}^{\text{II}}(\text{tpy})(\text{bpy})\text{OH}_2]^{2+}$  derivatives was first reported by Sakai's group<sup>13,32</sup> and extensively investigated by Berlinguette's group recently.<sup>15</sup> The established catalytic cycle for both examples includes formation of  $[\text{Ru}^{\text{V}}=\text{O}]$  species after stepwise ET steps and critical O–O bond formation through water nucleophilic attack to the  $\text{Ru}^{\text{V}}=\text{O}$  oxo group (also called 'acid–base' mechanism). Intriguing discoveries rise from comparison of catalytic kinetics between  $1^+$  and the previously published  $[\text{Ru}(\text{N}_3)(\text{N}_2)\text{L}]$  type of WOCs. At the same time, analysis of complex  $2^+$  under aqueous conditions allows us to re-examine the picoline/water ligand exchange that is believed to happen at the trivalent state of  $[\text{Ru}^{\text{II}}(\text{pdc})(\text{pic})_3]$  and  $[\text{Ru}^{\text{II}}(\text{hqc})(\text{pic})_3]$ .<sup>31</sup>

## EXPERIMENTAL SECTION

**Materials and Synthesis.** *cis*- $[\text{Ru}^{\text{II}}\text{Cl}_2(\text{dmsO})_4]$  and 6-methyl-2,2'-bipyridine were prepared according to published procedures.<sup>33</sup> Both 70%  $\text{HNO}_3$  (99.999% purity) and  $[\text{Ce}^{\text{IV}}(\text{NH}_4)_2](\text{NO}_3)_6$  (99.99% purity) were purchased from Sigma-Aldrich and used without further purification. Water used in both syntheses and measurements was deionized by Milli-Q technique. pH 1.0 nitric acid solution was prepared by diluting 70%  $\text{HNO}_3$  and calibrated by a pH meter (Metrohm 781). All other reagents and solvents are commercially available and used as received, unless otherwise noted.

**Synthesis of 2,2'-Bipyridine-6-carboxylic Acid (Hbpc).** To a solution of 6-methyl-2,2'-bipyridine (1 g, 5.8 mmol) in 20 mL of concentrated sulfuric acid at room temperature, 3.5 g (35 mmol) of  $\text{CrO}_3$  particle was slowly added under vigorous stirring. Addition of  $\text{CrO}_3$  was complete in about 45 min. The dark green mixture was kept at 70 °C for 4 h and then at room temperature for another 10 h. The reaction solution was then poured into 200 mL of ice water, affording a light yellow precipitate. The precipitate was filtrated, washed with water, and then dissolved in a NaOH solution (10%). The insoluble solid in the alkaline solution was removed by filtration. The filtrate was acidized to pH 1–2 by dropwise addition of 10% HCl, affording a milk white precipitate, which was collected, washed with water and ethanol, respectively, and dried under vacuum as the desired product (0.9 g, yield = 76%). <sup>1</sup>H NMR (500 MHz, *d*<sub>6</sub>-DMSO): 7.52 (dd, <sup>3</sup>J(H,H) = 7.0, 5.5 Hz, 1H), 8.02 (ddd, <sup>3</sup>J(H,H) = 7.5, 7.5 Hz, <sup>4</sup>J(H,H) = 1.5 Hz, 1H), 8.10–8.17 (m, 2H), 8.55 (d, <sup>3</sup>J(H,H) = 8.0 Hz, 1H), 8.60 (dd, <sup>3</sup>J(H,H) = 8.0 Hz, <sup>4</sup>J(H,H) = 1.0 Hz, 1H), 8.73 (d, <sup>3</sup>J(H,H) = 9.0 Hz, 1H).

**$[\text{Ru}^{\text{II}}(\text{bpy})(\text{dmsO})_2\text{Cl}_2]$ .** The complex was prepared according to the literature.<sup>34</sup> A solution of *cis*- $[\text{Ru}^{\text{II}}(\text{dmsO})_4\text{Cl}_2]$  (484 mg, 1 mmol) and bpy (156 mg, 1 mmol) in mixed EtOH (9 mL) and DMSO (1 mL) was refluxed for 1.5 h. After being allowed to cool to room temperature, the resulting orange precipitate was collected by filtration, washed with cold EtOH, and dried in vacuum (320 mg, yield = 66%). <sup>1</sup>H NMR of the product agrees with that described in the literature.

**$[\text{Ru}^{\text{II}}(\text{bpc})(\text{bpy})\text{Cl}]$ .** A solution of 2,2'-bipyridine-6-carboxylic acid (Hbpc, 100 mg, 0.5 mmol) and  $\text{Na}_2\text{CO}_3$  (53 mg, 0.5 mmol) in 2 mL of  $\text{H}_2\text{O}$  was added to a solution of  $[\text{Ru}^{\text{II}}(\text{bpy})(\text{dmsO})_2\text{Cl}_2]$  (242 mg, 0.5 mmol) in 10 mL of ethanol. The resulting mixture was completely degassed with  $\text{N}_2$  and then kept at 65 °C for 6 h under the protection of  $\text{N}_2$ . After being allowed to cool to room temperature, the solvent was removed by a rotary evaporator. The residue was then dissolved in 100 mL of dichloromethane and washed with water (50 mL × 2). The organic layer was dried by anhydrous  $\text{Na}_2\text{SO}_4$ , and then the dichloromethane was removed by a rotary evaporator. The raw product was further purified by column chromatography over silica using MeOH/ $\text{CH}_2\text{Cl}_2$  (gradient elution from 5/100 to 10/100) as

eluent. The desired product was attained as a dark red solid (145 mg, yield = 59%).  $^1\text{H}$  NMR (500 MHz,  $d_6$ -DMSO): 7.13–7.21 (m, 3H), 7.39 (d,  $^3J(\text{H,H}) = 5.5$  Hz, 1H), 7.73–7.78 (m, 2H), 7.92 (dd,  $^3J(\text{H,H}) = 6.5$ , 7.0 Hz, 1H), 8.02–8.05 (m, 2H), 8.15 (dd,  $^3J(\text{H,H}) = 7.5$ , 8.0 Hz, 1H), 8.56 (d,  $^3J(\text{H,H}) = 14.5$ , 1H), 8.59 (d,  $^3J(\text{H,H}) = 14.5$ , 1H), 8.74 (d,  $^3J(\text{H,H}) = 5.0$ , 1H), 8.80 (d,  $^3J(\text{H,H}) = 10.0$ , 1H), 10.13 (d,  $^3J(\text{H,H}) = 5.0$  Hz, 1H).  $^{13}\text{C}$  NMR (500 MHz,  $d_6$ -DMSO): 112.68, 112.78, 112.95, 123.40, 124.07, 125.70, 125.78, 126.21, 132.27, 133.96, 134.17, 134.67, 150.84, 152.35, 152.99, 154.35, 156.20, 157.17, 159.12, 159.31, 171.33.

$[\text{Ru}^{\text{II}}(\text{bpc})(\text{bpy})\text{OH}_2]^+\text{PF}_6^-$  ( $1^+\text{PF}_6^-$ ).  $[\text{Ru}^{\text{II}}(\text{bpc})(\text{bpy})\text{Cl}]$  (49 mg, 0.1 mmol) and  $\text{AgPF}_6$  (28 mg, 0.11 mmol) were combined in 5 mL of  $\text{MeOH}/\text{H}_2\text{O}$  (1:1) and kept stirring overnight at room temperature. The dark red mixture was then filtered through Celite to remove  $\text{AgCl}$ . Several drops of saturated  $\text{NH}_4\text{PF}_6$  solution were added to the filtrate, which was left standing in the fume hood for slow evaporation of  $\text{MeOH}$ . After about 24 h, small dark red crystals precipitate, which were collected by filtration, washed with cold water, and dried under vacuum, yielding 42 mg of desired complex (68%).  $^1\text{H}$  NMR (500 MHz,  $d_6$ -DMSO): 9.53 (d,  $^3J(\text{H,H}) = 5.5$  Hz, 1H), 8.88 (d,  $^3J(\text{H,H}) = 8.5$  Hz, 1H), 8.85 (d,  $^3J(\text{H,H}) = 8.0$  Hz, 1H), 8.66 (d,  $^3J(\text{H,H}) = 8.0$  Hz, 1H), 8.63 (d,  $^3J(\text{H,H}) = 8.0$  Hz, 1H), 8.26 (dd,  $^3J(\text{H,H}) = 7.5$ , 8.0 Hz, 1H), 8.19 (dd,  $^3J(\text{H,H}) = 7.5$ , 7.5 Hz, 1H), 8.12 (d,  $^3J(\text{H,H}) = 7.5$  Hz, 1H), 8.02 (dd,  $^3J(\text{H,H}) = 7.5$ , 7.5 Hz, 1H), 7.89 (dd,  $^3J(\text{H,H}) = 7.5$ , 7.5 Hz, 1H), 7.78 (dd,  $^3J(\text{H,H}) = 8.0$ , 7.5 Hz, 1H), 7.49 (d,  $^3J(\text{H,H}) = 5.5$  Hz, 1H), 7.28 (dd,  $^3J(\text{H,H}) = 5.5$ , 5.5 Hz, 1H), 7.19 (dd,  $^3J(\text{H,H}) = 5.0$ , 5.5 Hz, 1H), 7.16 (d,  $^3J(\text{H,H}) = 5.0$  Hz, 1H), 5.92 (s, 2H). Anal. Calcd for  $[\text{Ru}^{\text{II}}(\text{bpc})(\text{bpy})\text{OH}_2]^+(\text{PF}_6)^-\cdot 1.5\text{H}_2\text{O}$ : C, 39.02; H, 3.12; N, 8.67. Found: C, 39.36; H, 3.02; N, 8.41.

$[\text{Ru}^{\text{II}}(\text{bpc})(\text{pic})_3]^+\text{PF}_6^-$  ( $2^+\text{PF}_6^-$ ). To a solution of *cis*- $[\text{Ru}^{\text{II}}\text{Cl}_2(\text{dmsO})_4]$  (242 mg, 0.5 mmol) in 40 mL of methanol, a methanol solution containing 100 mg (0.5 mmol) of  $\text{Hbpc}$  and 0.5 mL of triethylamine was slowly added dropwise. After addition was complete, the resulting mixture was kept at 60 °C for 4 h. Then 1 mL of 4-picoline was added to the solution, and the mixture was gently refluxed for another 6 h. After being allowed to cool to room temperature, solvent was removed by a rotary evaporator. The black residue was dissolved in 10 mL of water. Addition of a saturated water solution of  $\text{NH}_4\text{PF}_6$  afforded a dark brown precipitate, which was collected by filtration and further purified by column chromatography over silica using  $\text{KNO}_3(\text{satd})/\text{H}_2\text{O}/\text{acetonitrile}$  (0.1/2/100) as eluent. The desired product was attained as a dark brown solid (115 mg, yield = 32%) after  $\text{NO}_3^-$  was replaced by  $\text{PF}_6^-$ .  $^1\text{H}$  NMR (500 MHz,  $\text{CDCl}_3$ ): 2.22 (s, 6H), 2.47 (s, 3H), 6.85 (d,  $^3J(\text{H,H}) = 6.5$  Hz, 4H), 7.28 (d,  $^3J(\text{H,H}) = 6.0$  Hz, 2H), 7.55 (d,  $^3J(\text{H,H}) = 6.5$  Hz, 4H), 7.78 (dd,  $^3J(\text{H,H}) = 8.0$ , 7.0 Hz, 1H), 7.85 (dd,  $^3J(\text{H,H}) = 6.5$ , 6.5 Hz, 1H), 7.93 (dd,  $^3J(\text{H,H}) = 8.0$ , 7.5 Hz, 1H), 8.10 (d,  $^3J(\text{H,H}) = 7.5$  Hz, 1H), 8.21 (dd,  $^3J(\text{H,H}) = 9.0$  Hz, 2H), 8.32 (d,  $^3J(\text{H,H}) = 6.5$  Hz, 2H), 8.88 (d,  $^3J(\text{H,H}) = 5.5$  Hz, 1H).  $^{13}\text{C}$  NMR (500 MHz,  $\text{CDCl}_3$ ): 20.78, 21.13, 123.33, 123.43, 125.96, 126.29, 127.21, 129.38, 132.82, 136.29, 147.50, 148.89, 149.41, 151.53, 153.32, 154.87, 155.93, 158.91, 173.10. Anal. Calcd for  $[\text{Ru}^{\text{II}}(\text{bpc})\text{pic}_3]^+\text{PF}_6^-\cdot 1.8\text{H}_2\text{O}$ : C, 46.01; H, 4.21; N, 9.25. Found: C, 46.56; H, 4.074; N, 8.740.

**Physical Methods.**  $^1\text{H}$  and  $^{13}\text{C}$  NMR spectroscopies were conducted on a Bruker Advance 500 Hz nuclear magnetic resonance spectrometer. UV–vis absorption spectra were measured by a PerkinElmer Lambda 750 UV–vis spectrophotometer. Elemental analyses were performed with a Thermoquest-Flash EA 1112 apparatus. Electrochemical measurements, including cyclic voltammetry (CV) and differential pulse voltammetry (DPV), were carried out under aerobic conditions and recorded with an Autolab potentiostat and a GPES electrochemical interface (Eco Chemie) using a glassy carbon disk (diameter = 3 mm) as the working electrode, a platinum wire as the counter electrode, and a saturated calomel electrode (SCE) as the reference electrode. At  $\text{pH} \leq 1.0$ , the  $\text{HNO}_3$  solution was employed as electrolyte. Otherwise, the electrolytes used were a series of phosphate buffers (ionic strength = 0.1 M), of which  $\text{pH}$  was adjusted by addition of trifluoromethanesulfonic acid or  $\text{NaOH}$  solution.  $[\text{Ru}^{\text{II}}(\text{bpy})_3]\text{Cl}_2$  ( $E^{1/2}(\text{Ru}^{\text{III}}/\text{Ru}^{\text{II}}) = 1.26$  V vs NHE

in aqueous medium) was used as an external standard, and potentials reported herein were referenced to NHE.

Kinetic studies on the stepwise oxidation of Ru complexes were performed by a stopped-flow module Bio-Logic SFM300 coupled with a xenon light source and a fast JM TIDAS UV–vis Diode Array spectrophotometer. Spectral changes were detected in the wavelength range of 300–700 nm. The temperature during measurements was maintained by a thermostatted bath (Polystate 36, Fisher Scientific). Rate constants of single-step reactions were calculated by a single-wavelength fitting or global fitting according to the rate-law algorithm within ReactLab KINETICS (Version 1.1) software.

Initial rates of  $\text{O}_2$  generation of  $\text{Ce}^{\text{IV}}$ -driven water oxidation at different catalyst concentrations were measured with a pressure transducer (Omega PX138-030A5 V) driven at 8.00 V (power supply TTi-PL601) and a data acquisition module (Omega OMB-DAQ-2416; running at 2 Hz for our measurements). In a typical run, a 25 mL round-bottomed flask was charged with 3.2 mL of a  $\text{Ce}^{\text{IV}}/\text{HNO}_3$  aqueous solution (0.083 mM,  $\text{pH} = 1.0$ ) and a certain amount of catalyst in  $\text{HNO}_3$  solution ( $\text{pH} 1.0$ ) was injected into the  $\text{Ce}^{\text{IV}}$  solution through a septum cap. At the end of each measurement, a gas sample was purged into the gas chromatography (GC-2014, SHIMADZU) for determination of the amount of the evolved  $\text{O}_2$ .

Two MS instruments were used to capture intermediates involved in catalytic water oxidation. One is a Finnigan LCQ Advantage MAX mass spectrometer equipped with atmospheric-pressure chemical ionization (APCI) source, and the experimental parameters were as follows: source voltage, 4.95 kV; capillary temperature, 175 °C; capillary voltage, 29.64 V; sheath gas flow rate, 3.76 L/h; tube lens voltage, 15.00 V. The other is a Bruker MicroTOF mass spectrometer equipped with an electrospray ionization (ESI) source, and the experimental parameters were as follows: capillary temperature, 180 °C; capillary voltage, 4500 V; flow rate, 4 L/min; capillary exit, 160 V; skimmer, 53.3 V; hexapole, 24 V.

The  $\text{HNO}_3$  solution ( $\text{pH} 2.0$ ) of catalyst and  $\text{Ce}^{\text{IV}}$  was mixed in a glass vial under vigorous stirring, and the resulting sample was directly injected into the MS by a syringe.

X-ray-quality single crystals of  $1^+$  and  $2^+$  were obtained from slow evaporation of their  $\text{CH}_3\text{OH}/\text{H}_2\text{O}$  solutions and single crystals of  $[\text{Ru}^{\text{II}}(\text{bpc})(\text{bpy})\text{Cl}]$  from its  $\text{CH}_2\text{Cl}_2/\text{heptane}$  solution thereof. Single-crystal X-ray diffraction data were collected on an Oxford Xcalibur 3 with molybdenum radiation ( $\lambda = 0.71073$  Å). Data reduction and absorption correction were applied with CrysAlis. Structures were solved by direct methods with SHELXS97, and all non-hydrogen atoms were refined with anisotropic displacement parameters with SHELXL97 using a full-matrix least-squares technique on  $F^2$ .<sup>35</sup> All hydrogen atoms were found in the Fourier difference maps in complexes  $1^+$  and  $[\text{Ru}^{\text{II}}(\text{bpc})(\text{bpy})\text{Cl}]$  including those of the water molecules, while hydrogen atoms were fixed to parent atoms using a riding model for complex  $2^+$ . Data resolution for  $2^+$  was cut at 0.80 Å due to weak intensities of reflections at higher  $2\theta$  values.

## RESULTS

**Synthesis, Characterization, and Structure.** *cis*- $[\text{Ru}^{\text{II}}(\text{dmsO})_4\text{Cl}_2]$  was used as a precursor for syntheses of both complexes  $1^+$  and  $2^+$ . The synthesis method was developed upon the chemical property of *cis*- $[\text{Ru}^{\text{II}}(\text{dmsO})_4\text{Cl}_2]$ , of which four dmsO ligands can be replaced stepwise under different reaction conditions.<sup>36</sup> In the case of complex  $1^+$ , two dmsO of  $[\text{Ru}^{\text{II}}(\text{dmsO})_4\text{Cl}_2]$  were first replaced by bpy, affording  $[\text{Ru}^{\text{II}}(\text{bpy})(\text{dmsO})_2\text{Cl}_2]$ ,<sup>34</sup> the other two dmsO and one  $\text{Cl}^-$  were subsequently replaced by  $\text{bpc}^-$ , affording  $[\text{Ru}^{\text{II}}(\text{bpc})(\text{bpy})\text{Cl}]$ , and finally  $1^+$  was obtained by replacing the left  $\text{Cl}^-$  with  $\text{H}_2\text{O}$  in the presence of  $\text{Ag}^+$ . Both  $[\text{Ru}^{\text{II}}(\text{bpy})(\text{dmsO})_2\text{Cl}_2]$  and  $[\text{Ru}^{\text{II}}(\text{bpc})(\text{bpy})\text{Cl}]$  were isolated and characterized as intermediates. In the case of complex  $2^+$ , *cis*- $[\text{Ru}^{\text{II}}(\text{dmsO})_4\text{Cl}_2]$  was treated with 1 equiv of  $\text{bpc}$  and excess 4-picoline successively in an one-pot reaction, and  $2^+$  was afforded by

stepwise self-assembly of the ruthenium core with bpc and pic ligands.

1D and 2D NMR experiments were conducted to characterize the complexes (see Experimental Section and Figures S1–S7, Supporting Information). Their coordinated bpc and bpy ligands exhibited an independent, well-resolved 1D proton resonance with ABC and AB spin coupling, and assignment of each signal could be accomplished with the assistance of 2D correlation spectroscopy (COSY). A benchmark used in the analysis of NMR spectra was the 6'-H of bpy (Figure S7, Supporting Information), which was considerably sensitive to its vicinal coordination environment. Its signal usually appears as a doublet peak with the largest downfield shift in the spectrum, due to a strong deshielding effect of nearby chloride or water ligated to the Ru center.<sup>11,16</sup> The two axial picolines of  $2^+$  were equivalent and showed one pair of 4H doublets peaks in the downfield, assigned to the ortho and meta protons of the picoline ring, respectively. This indicated a  $C_s$  symmetry of  $2^+$  in solution state with a reflection plane containing the tridentate bpc ligand.

The  $^1\text{H}$  NMR spectral profile of  $1^+$  in  $d_6$ -dmsO changed over time, reflecting conversion of  $1^+$  to another species under the NMR conditions (Figure S7, Supporting Information). A distinctive difference between the initial spectrum and that after 3 h, within which conversion was accomplished, was disappearance of the resonance signal at  $\delta = 5.92$  ppm corresponding to protons of the aqua ligand of  $1^+$ . All other peaks kept their integrations and spin coupling patterns but experienced downfield or upfield shifts in different extents. On the basis of these observations, substitution of the aqua ligand by a dmsO molecule was inferred to occur when  $1^+$  was dissolved in dmsO. Because the dmsO donor, rather than  $\text{H}_2\text{O}$ , had a more significant deshielding influence over the 6'-H of bpy, an obvious downfield shift of its resonance was expected after the  $\text{H}_2\text{O}/\text{dmsO}$  exchange. This expectation was consistent with the experimental result that is a shift of the doublet peak from  $\delta = 9.53$  to 10.15 ppm. NMR of  $1^+$  in other common deuterium solvents was not performed due to its inadequate solubility. Displacement of the chloro ligand in a  $d_6$ -dmsO solution of  $[\text{Ru}^{\text{II}}(\text{bpc})(\text{bpy})\text{Cl}]$  was not observed by NMR over a 6 h period.

X-ray crystal structures of  $1^+\text{PF}_6^-$ ,  $2^+\text{PF}_6^-$ , and  $[\text{Ru}^{\text{II}}(\text{bpc})(\text{bpy})\text{Cl}]$  are presented in Figure 1 and Figure S8, Supporting Information; selected crystallographic parameters are listed in Table 1 and Tables S1 and S2, Supporting Information. In all cases, the Ru center adopts a distorted octahedral geometry of which three positions are occupied by the tridentate bpc ligand. Other notable features include the following: (i) the bond distances from the Ru center of  $1^+$  to the two nitrogen atoms of bpy are significantly different (by 0.05 Å), with a shorter Ru1–N4 bond trans to the aqua ligand (2.016(2) Å); (ii) the bond distances from Ru center of  $2^+$  to its three picoline nitrogen atoms are slightly different, with the longest Ru1–N3 bond (2.120 Å) at the opposite position of bpc. These phenomena can be explained by electronic effects between ligands and Ru as well as steric interaction among ligands.<sup>37</sup> Furthermore, the Ru–N(bpy) bonds (2.016–2.066 Å) of  $1^+$  are much shorter than the Ru–N(picoline) bonds (2.092–2.120 Å) of  $2^+$ , indicating a stronger coordination between Ru and bpy.

Compared to the crystal structure of  $[\text{Ru}^{\text{II}}(\text{tpy})(\text{bpy})\text{OH}_2]^{2+}$ ,<sup>37</sup> the corresponding Ru1–O3(aqua) and Ru–N(bpy) bonds of  $1^+$  are considerably longer due to the cis effect of the carboxylate group. This effect also elongates Ru–N(picoline)

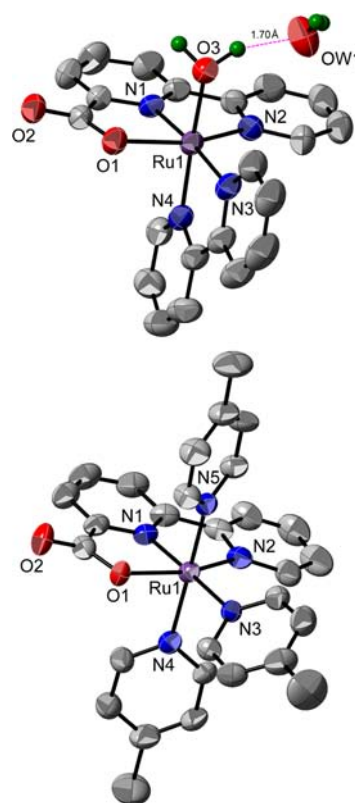


**Figure 1.** X-ray crystal structures of  $1^+\text{PF}_6^-$  (top, ellipsoids at 40% probability) and  $2^+\text{PF}_6^-$  (bottom, ellipsoids at 40% probability); hydrogen atoms (except water) and  $\text{PF}_6^-$  are omitted for clarity; color code: ruthenium (purple), nitrogen (blue), oxygen (red), carbon (gray) and hydrogen (green).

**Table 1.** Selected Bond Distances (Angstroms) and Angles (degrees) for  $1^+\text{PF}_6^-$  and  $2^+\text{PF}_6^-$

	1	2	
bond distances			
Ru1–N1	1.959(2)	Ru1–N1	1.950(4)
Ru1–N2	2.032(3)	Ru1–N2	2.059(4)
Ru1–N3	2.066(2)	Ru1–N3	2.120(4)
Ru1–N4	2.016(2)	Ru1–N4	2.111(4)
Ru1–O1	2.125(2)	Ru1–N5	2.092(4)
Ru1–O3	2.112(2)	Ru1–O1	2.111(3)
HOA–OW1	1.70(2)		
bond angles			
N3–Ru1–O3	90.53(9)	N2–Ru1–O1	159.6(1)
N2–Ru1–O3	92.65(9)	N5–Ru1–N4	176.2(1)
N4–Ru1–O1	158.38(8)	N1–Ru1–N4	89.3(1)
N1–Ru1–N2	78.90(9)	N3–Ru1–N4	88.6(1)

bonds of  $2^+$ , which will be elaborated in the next section. A hydrogen bond between solvated  $\text{H}_2\text{O}$  and coordinative carboxylate was observed in the crystal of  $[\text{Ru}^{\text{II}}(\text{bpc})(\text{bpy})\text{Cl}]$ . Similar hydrogen bonding at the carbonyl groups of complexes  $1^+$  and  $2^+$  is expected in their aqueous solutions. Theoretical studies have found that a proton acceptor near the active site of a Ru WOC favors the proton-coupled electron-transfer (PCET) process, through which high-valent Ru species were accessed.<sup>31,38,39</sup>

UV–vis spectra of  $1^+$  and  $2^+$  in pH 1.0  $\text{HNO}_3$  were displayed in Figures S9 and S10, Supporting Information. Neither of their absorption profiles showed a discernible change over a 2 h

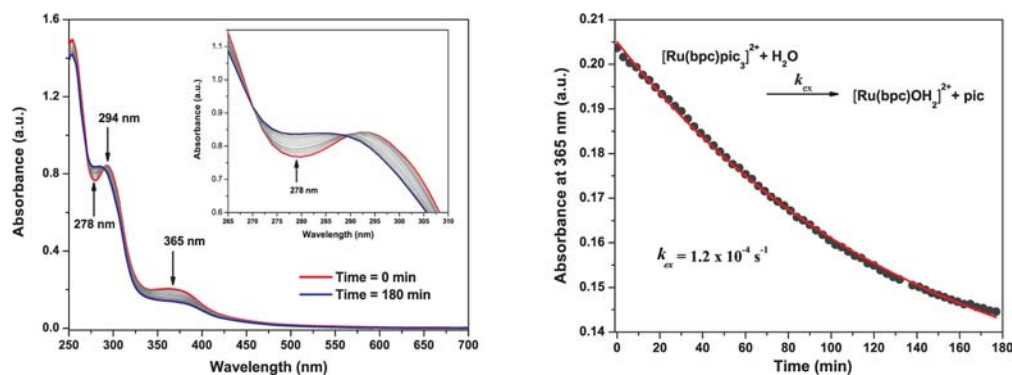


**Figure 2.** Kinetics study of the  $\text{H}_2\text{O}/\text{pic}$  exchange. (Left) Absorbance change of  $2^{2+}$  (0.05 mM) in  $\text{HNO}_3$  (pH 1.0) over 180 min;  $2^{2+}$  was achieved by oxidizing  $2^{1+}$  with 1 equiv of  $\text{Ce}^{\text{IV}}$ ; (insert) enlarged part from 265 to 310 nm. (Right) Fitting of the time profile of absorbance at 358 nm by first-order reaction law.

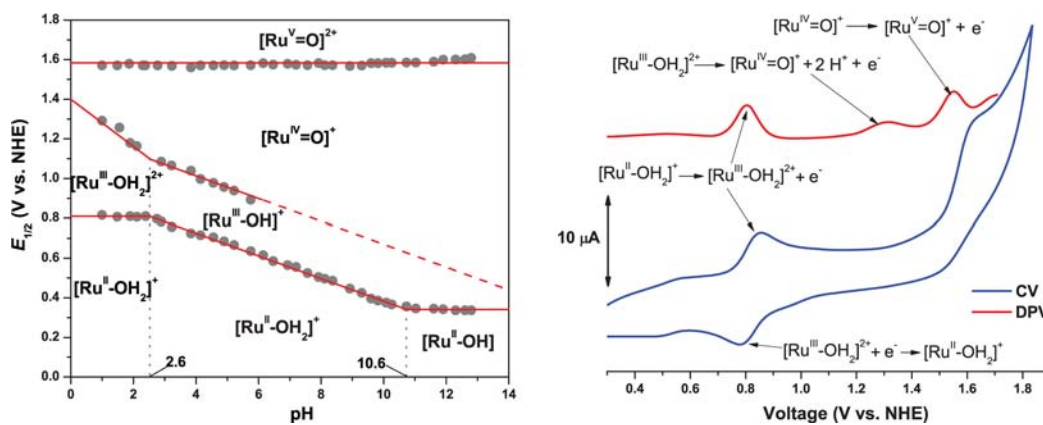


**Figure 3.** Electrochemical behavior of  $1^+$ . (Left) Pourbaix diagram for  $1^+$ : red lines indicate trends of redox potentials ( $E_{1/2}$ ) depending on pH values; gray dots are redox events observed. (Right) Cyclic voltammogram for  $1^+$  in pH 1.0  $\text{HNO}_3$  (blue, scan rate, 100 mV/s); differential pulse voltammetry for  $1^+$  in pH 1.0  $\text{HNO}_3$  (red, step potential = 5 mV, amplitude = 25 mV, frequency = 10  $\text{s}^{-1}$ , modulation time = 0.05 s).

period, indicative of the proper stability of  $1^+$  and  $2^+$  in acidic solution. In either situation, two separate metal-to-ligand charge transfer (MLCT) absorbance bands were observed: one appeared at around 480 nm corresponding to a  $\text{Ru}(d\pi) \rightarrow \text{bpc}(p\pi^*)$  transition and the other at around 350 nm corresponding to the  $\text{Ru}(d\pi) \rightarrow \text{bpy}/\text{pic}(p\pi^*)$  transition. The local  $\text{bpc}(p\pi) \rightarrow \text{bpc}(p\pi^*)$  transition arose at about 290 nm as the most intense band in either spectrum.

The  $\text{p}K_{\text{a}}$  value of  $1^+$  was determined to be 10.6 by titration in a phosphate buffer (Figures S11 and S12, Supporting Information). As the pH value rises from 7.5 to 12.5, MLCT bands in the UV-vis spectrum of  $1^+$  shift evidently toward the longer wavelength, from 350 and 488 nm to 375 and 522 nm respectively, because the hydroxyl group resulting from deprotonation is a stronger  $\delta$ -donating ligand than the originally coordinative aqua ligand.

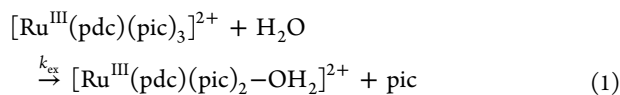
**Ligand Exchange.** We described above that the  $\text{Ru}^{\text{II}}-\text{OH}_2$  bond of  $1^+$  is weak, and the aqua ligand could be replaced by dmso. Meyer et al. verified that  $[\text{Ru}(\text{N}_3)(\text{N}_2)\text{OH}_2]$  type of complexes also undergo water/solvent ligand exchange in the presence of coordinative organic solvents such as acetonitrile and 2,2,2-trifluoroethanol.<sup>40</sup> The  $\text{Ru}$ -solvent and  $\text{Ru}-\text{OH}_2$  species usually exist in dynamic equilibrium, of which the constants are determined by the nature of the organic solvent. Involvement of ligand exchange may complicate the spectroscopic behavior of  $\text{Ru}$  complexes<sup>31</sup> and suppress their catalytic activity because of an inaccessible PCET process. Conse-

quently, any organic solvents with coordinating ability were avoided as far as possible in the study of  $1^+$  and  $2^+$ .

Our previous work has revealed that one pic ligand of  $[\text{Ru}^{\text{II}}(\text{pdc})(\text{pic})_3]$  was readily replaced by  $\text{H}_2\text{O}$  when it was oxidized to the  $\text{Ru}^{\text{III}}$  state.<sup>31</sup> Theoretical calculations suggest that ligand exchange happens through a dissociative pathway via a five-coordinated intermediate. Compared to neutral tpy ligand, anionic pdc ligand can better stabilize the intermediate and thus remarkably reduce the energy barrier of the ligand-dissociation process.<sup>31</sup> This labile effect of anionic ligands can be explained primarily from the electron-donating effect of the carboxylate donor.<sup>41</sup> In principle, the anionic oxygen atom can donate an extra pair of electrons from its p orbital to the electron-deficient  $\text{Ru}$  center of the coordinatively unsaturated intermediate so as to stabilize the intermediate. Likewise, this labile effect might also favor liberation of  $\text{O}_2$  from ruthenium peroxo species, which is believed to be the rate-determining step in the catalytic cycle of some  $[\text{Ru}(\text{N}_3)(\text{N}_2)\text{L}]$  WOCs.<sup>10,15,21</sup>

In the current work, we investigated the lability of the  $\text{Ru}^{\text{III}}-\text{N}(\text{pic})$  bond of  $2^{2+}$  in aqueous solution. The trivalent  $\text{Ru}$  complex  $2^{2+}$  was attained by mixing equimolar  $2^+$  and  $\text{Ce}^{\text{IV}}$  in pH 1.0  $\text{HNO}_3$ . The resulting UV-vis spectral profile of  $2^{2+}$  showed increasing absorbance at 365 and 278 nm and decreasing absorbance at 294 nm over 3 h (Figure 2). Two isosbestic points at 270 and 290 nm were clearly observed in the time-resolved spectra, indicating emergence of a new

species. Taking our previous findings into account, we speculated that  $2^{2+}$  proceeded with a  $\text{H}_2\text{O}/\text{pic}$  ligand exchange (eq 1) via a dissociative pathway similar to that of  $[\text{Ru}^{\text{III}}(\text{pdc})(\text{pic})_3]^{2+}$



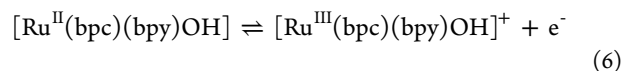
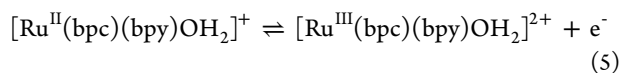
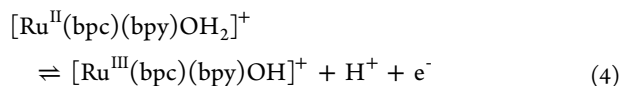
$$\frac{d[\text{Ru}^{\text{III}}(\text{bpc})(\text{pic})_3]^{2+}}{dt} = -k_{\text{ex}}[\text{Ru}^{\text{III}}(\text{bpc})(\text{pic})_3]^{2+} \quad (2)$$

$$\ln\left(\frac{A - A_{\infty}}{A_0 - A_{\infty}}\right) = -k_{\text{ex}}t \quad (3)$$

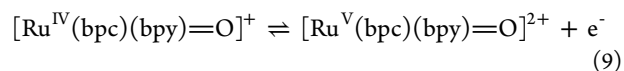
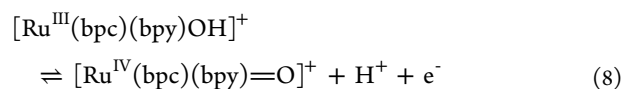
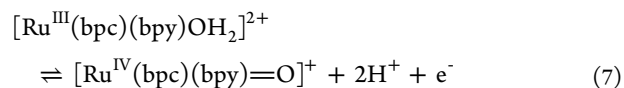
Kinetics of this ligand exchange for  $2^{2+}$  follows a pseudo-first-order rate law described in eq 2. Equation 3 is an integrated expression of the rate law in terms of spectroscopic absorbance, where  $A$ ,  $A_0$ , and  $A_{\infty}$  represent absorbance at time  $t$ , 0, and infinity, respectively. The rate constant  $k_{\text{ex}} = 1.2 \times 10^{-4} \text{ s}^{-1}$  was obtained by fitting the trace of absorbance decay at 365 nm (Figure 2) according to eq 3. In principle,  $[\text{Ru}^{\text{III}}(\text{pdc})(\text{pic})_3]^{2+}$  should own a greater rate constant of ligand exchange under the same conditions owing to the double carboxylate groups of pdc.

**Electrochemical Behavior.** The differential pulse voltammetry (DPV) curve of  $1^+$  in acidic aqueous condition (pH 1.0  $\text{HNO}_3$ ) exhibits a sequence of three current signals at 0.81, 1.29, and 1.57 V vs NHE (Figure 3), corresponding to redox potentials  $E^{1/2}(\text{Ru}^{\text{III}}/\text{Ru}^{\text{II}})$ ,  $E^{1/2}(\text{Ru}^{\text{IV}}/\text{Ru}^{\text{III}})$ , and  $E^{1/2}(\text{Ru}^{\text{V}}/\text{Ru}^{\text{IV}})$ , respectively. The cyclic voltammogram of  $1^+$  under the same conditions reveals an onset of rapid current increase at around 1.6 V vs NHE owing to catalytic water oxidation, which partially overlaps with the quasi-reversible wave of the  $\text{Ru}^{\text{V}}/\text{Ru}^{\text{IV}}$  redox process. Under a neutral aqueous condition (pH 7.1 phosphate buffer), the CV curve of  $1^+$  shows a more significant catalytic current that also initiates along with the  $\text{Ru}^{\text{V}}/\text{Ru}^{\text{IV}}$  redox event at about 1.6 V vs NHE (Figure S13, Supporting Information). The reversible  $\text{Ru}^{\text{III}}/\text{Ru}^{\text{II}}$  redox wave of  $1^+$  appears at more cathodic position (0.56 V vs NHE) in pH 7.1 buffer than that in pH 1.0  $\text{HNO}_3$ .

The Pourbaix diagram of  $1^+$  (Figure 3) provides comprehensive information about the predominant redox compositions depending on the voltage potentials and the pH of the surroundings. The  $\text{p}K_{\text{a}}$  of  $[\text{Ru}^{\text{II}}(\text{bpc})(\text{bpy})\text{OH}_2]^+$  determined from its Nernstian behavior is 10.6, which agrees with the result from spectrophotometric titration in phosphate buffer (vide supra), and the  $\text{p}K_{\text{a}}$  of  $[\text{Ru}^{\text{III}}(\text{bpc})(\text{bpy})\text{OH}_2]^{2+}$  determined is 2.6. In the region from pH = 2.6 to 10.8,  $E^{1/2}(\text{Ru}^{\text{III}}/\text{Ru}^{\text{II}})$  decreases linearly with a slope of ca.  $-59 \text{ mV/pH}$ . This phenomenon is evoked by a typical one-electron and one-proton PCET process described in eq 4. In the region of pH > 10.6 or < 2.6, the redox potential of  $\text{Ru}^{\text{III}}/\text{Ru}^{\text{II}}$  remains independent in pH changes, which reflects a one-electron transfer process expressed in eqs 5 and 6, respectively.



For the potentials of  $\text{Ru}^{\text{IV}}/\text{Ru}^{\text{III}}$  redox couples, a slope of ca.  $-118 \text{ mV/pH}$  is observed in the strong acidic region (pH < 2.6), which corresponds to formation of  $[\text{Ru}^{\text{IV}}=\text{O}]^+$  species via a coupled two-proton and one-electron transfer (eq 7). At pH > 2.6,  $[\text{Ru}^{\text{IV}}(\text{bpc})(\text{bpy})=\text{O}]^+$  is supposed to come from  $[\text{Ru}^{\text{III}}(\text{bpc})(\text{bpy})\text{OH}]^+$  via a one-proton and one-electron PCET process (eq 8). While we indeed observed a  $[\text{Ru}^{\text{IV}}=\text{O}]^+ / [\text{Ru}^{\text{III}}-\text{OH}]^+$  redox signal shifting by approximately  $-59 \text{ mV}$  per pH over the range from pH = 2.6 to 6.0, this  $[\text{Ru}^{\text{IV}}=\text{O}]^+ / [\text{Ru}^{\text{III}}-\text{OH}]^+$  redox event became a too broad and weak wave to be distinguished at pH > 6.0; no matter wave or DPV electrochemical technique was applied. This result is probably triggered by slow kinetics of the redox process ( $[\text{Ru}^{\text{IV}}=\text{O}]^+ / [\text{Ru}^{\text{III}}-\text{OH}]^+$ ) at the working electrode. Further oxidation of  $[\text{Ru}^{\text{IV}}=\text{O}]^+$  species to the formal  $[\text{Ru}^{\text{V}}=\text{O}]^{2+}$  complex occurs at a relatively constant potential of 1.58 V vs NHE over the pH 1–13 range (eq 9).



The electrochemical property of complex  $2^+$  is quite different from that of  $1^+$ . In principle, the saturated, nonaqua coordinate motif of  $2^+$  cannot access a high-valent state via PCET. In a pH 1.0 solution of  $2^+$ , equilibrium of  $[\text{Ru}^{\text{II}}(\text{bpc})(\text{pic})_3]^{2+} / [\text{Ru}^{\text{III}}(\text{bpc})(\text{pic})_3]^{2+}$  at 0.89 V vs NHE was the only redox event observed in a 0–1.6 V (vs NHE) potential sweep window (Figure S14, Supporting Information). Otherwise, in a pH 1.0 solution of  $2^{2+}$  where  $2^+$  was oxidized to  $\text{Ru}^{\text{III}}$  state by addition of 1 equiv of  $\text{Ce}^{\text{IV}}$ , the  $[\text{Ru}^{\text{II}}(\text{bpc})(\text{pic})_3]^{2+} / [\text{Ru}^{\text{III}}(\text{bpc})(\text{pic})_3]^{2+}$  wave shrunk evidently over 3 h and a new redox signal at about 0.62 V vs NHE was rising during the same time period (Figure 4 and Figure S14, Supporting Information). This emerging wave was attributed to the presence of  $[\text{Ru}^{\text{III}}(\text{bpc})(\text{pic})_2\text{OH}_2]^{2+} / [\text{Ru}^{\text{II}}(\text{bpc})(\text{pic})_2\text{OH}_2]^+$  redox couples resulting from  $\text{pic}/\text{H}_2\text{O}$  ligand exchange happening to  $[\text{Ru}^{\text{III}}(\text{bpc})-$

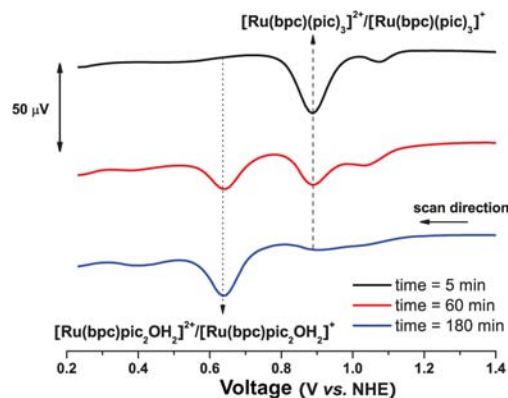


**Figure 4.** DPV of  $2^{2+}$  (0.5 nM) after different time durations;  $2^+$  was oxidized by addition of 1 equiv of  $\text{Ce}^{\text{IV}}$  at  $t = 0 \text{ min}$ .

(pic)<sub>3</sub>]<sup>2+</sup> (vide supra). There is another redox wave at ca. 1.1 V, of which the strength is attenuating over time. It should not derive from the aqua–Ru<sup>III</sup> species generated from ligand exchange. Otherwise, the strength of the wave would be rising with the growth of the [Ru<sup>III</sup>(bpc)(pic)<sub>2</sub>OH<sub>2</sub>]<sup>2+</sup>/[Ru<sup>II</sup>(bpc)(pic)<sub>2</sub>OH<sub>2</sub>]<sup>+</sup> wave contemporarily. Without the presence of Ce<sup>IV</sup>, no redox signal at 1.1 V was observed in the potential sweep experiments of 2<sup>+</sup>. Intuitively, this anomalous wave is ascribed to some cerium species which has not been clearly delineated yet.

Under neutral conditions (pH 7.1 phosphate buffer), the [Ru<sup>II</sup>(bpc)(pic)<sub>3</sub>]<sup>+</sup>/[Ru<sup>III</sup>(bpc)(pic)<sub>3</sub>]<sup>2+</sup> redox process appeared at 0.89 V, the same as that in acidic medium. However, the pic/H<sub>2</sub>O ligand exchange of 2<sup>+</sup> was accelerated apparently in the neutral aqueous medium, and the aqua complex can generate in situ during the potential sweep from 0 to 1.6 V vs NHE (Figure S15a, Supporting Information). The redox wave appearing at 0.49 V vs NHE is assigned to be the potential of [Ru<sup>III</sup>(bpc)(pic)<sub>2</sub>OH]<sup>+</sup>/[Ru<sup>II</sup>(bpc)(pic)<sub>2</sub>OH<sub>2</sub>]<sup>+</sup> redox couples. There are two pieces of electrochemical evidence supporting this conclusion. One is that the strength of reversible redox waves at 0.49 V was substantially restrained when the scan rate of CV was increased from 100 to 1000 mV s<sup>-1</sup> (Figure S15b and S15c, Supporting Information). The other is that the assigned potential of the aqua–Ru<sup>III</sup>/Ru<sup>II</sup> redox couples at pH 7.1—0.49 V is lower than that at pH 1.0, reflecting a Nernstian effect upon PCET. In addition, catalytic current from water oxidation was also observed in the potential sweep measurement. Meanwhile, we also found that the [Ru<sup>III</sup>(bpc)(pic)<sub>2</sub>OH]<sup>+</sup>/[Ru<sup>II</sup>(bpc)(pic)<sub>2</sub>OH<sub>2</sub>]<sup>+</sup> redox signal appeared during DPV sweep from the anodic to the cathodic direction (1.1 → 0.2 V vs NHE) but not in the reverse direction (0.2 → 1.1 V, Figure S15d, Supporting Information). This finding corroborated the occurrence of pic/H<sub>2</sub>O ligand exchange after formation of trivalent Ru species, as we described above and previously.<sup>31</sup>

**Dioxygen Evolution.** The catalytic O<sub>2</sub>-evolving ability of complexes 1<sup>+</sup>PF<sub>6</sub><sup>-</sup> and 2<sup>+</sup>PF<sub>6</sub><sup>-</sup> were evaluated in pH 1.0 HNO<sub>3</sub> containing a large excess of Ce<sup>IV</sup> (1500–5500 equiv) as an electron acceptor. The amount of generated dioxygen was monitored using a pressure transducer and calibrated by GC at the end of each measurement. Under this catalytic condition, the initial O<sub>2</sub>-evolving rate is irrelevant to the concentration of Ce<sup>IV</sup>, which can be regarded as a constant with respect to the concentration of the catalyst.

As soon as an aqueous solution of 1<sup>+</sup>PF<sub>6</sub><sup>-</sup> was injected into the HNO<sub>3</sub>–Ce<sup>IV</sup> medium, instant O<sub>2</sub> generation was detected (Figure 5). In addition, the initial rate of O<sub>2</sub> evolution (over 0–300 s) was found to be proportional to the initial concentration of 1<sup>+</sup>, following a pseudo-first-order expression initial rate = k<sub>O<sub>2</sub></sub>[1<sup>+</sup>] (Figure 5). The calculated rate constant k<sub>O<sub>2</sub></sub> = 0.165 s<sup>-1</sup> for 1<sup>+</sup> that is equal to its turnover frequency (TOF) is approximately one order in magnitude higher than that of [Ru<sup>II</sup>(tpy)(bpy)OH<sub>2</sub>]<sup>2+</sup> and remarkably higher than those of [Ru<sup>II</sup>(tpy)(bpy)OH<sub>2</sub>]<sup>2+</sup> derivatives.<sup>13,15,42</sup> Nevertheless, the O<sub>2</sub> evolution mediated by 1<sup>+</sup> became sluggish as the reaction proceeded (Figure S16, Supporting Information) and almost stopped after 1 h of catalysis, when Ce<sup>IV</sup> in the solution was not completely consumed yet. This inactivation illustrates decomposition of 1<sup>+</sup> under the harshly oxidizing HNO<sub>3</sub>–Ce<sup>IV</sup> conditions. The turnover number (TON) of 1<sup>+</sup> was measured as 540 after 1 h reaction.

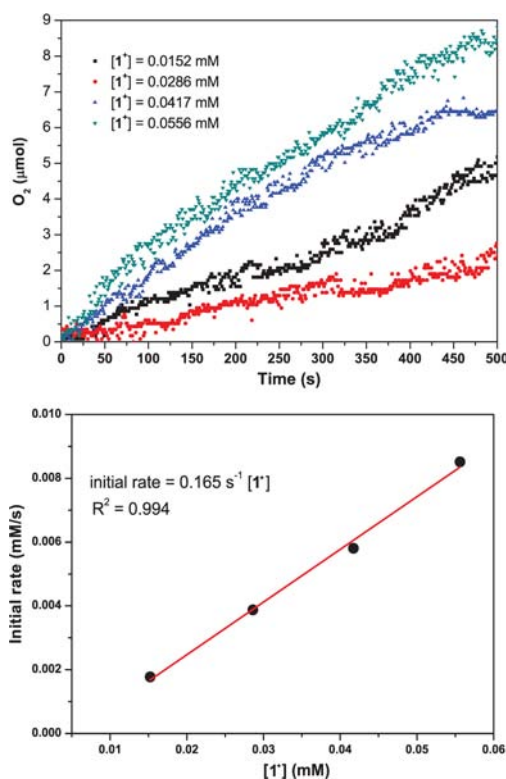
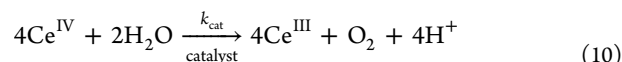


**Figure 5.** Kinetics of O<sub>2</sub> evolution for 1<sup>+</sup>PF<sub>6</sub><sup>-</sup>. (Top) Plots of O<sub>2</sub> evolution vs time at various concentrations of catalyst 1<sup>+</sup> in pH 1.0 HNO<sub>3</sub> (3 mL) containing Ce<sup>IV</sup> (0.083 M). Initial rates were calculated by fitting the O<sub>2</sub> vs time curves from 0 to 300 s as a straight line. (Bottom) Determination of k<sub>O<sub>2</sub></sub> by plotting the initial rate of O<sub>2</sub> generation against the concentration of 1<sup>+</sup>. Initial rate of O<sub>2</sub> output is normalized to the volume of solution present in the experiment.

Introduction of 2<sup>+</sup> into the HNO<sub>3</sub>–Ce<sup>IV</sup> solution did not trigger instant O<sub>2</sub> evolution. Induction periods from tens to hundreds of seconds depending on the initial concentration of 2<sup>+</sup> were observed before a satisfactory signal-to-noise O<sub>2</sub> level was verified (Figure S17, Supporting Information). This induction time corresponds to the pic/H<sub>2</sub>O ligand exchange process which is prerequisite for formation of an aqua species, [Ru<sup>III</sup>(bpc)(pic)<sub>2</sub>OH<sub>2</sub>]<sup>2+</sup>, as the authentic WOC mediating O<sub>2</sub> evolution. A much longer induction time (>2 h) has been observed for [Ru<sup>II</sup>(tpy)(pic)<sub>3</sub>]<sup>2+</sup> but none for [Ru<sup>II</sup>(pdc)(pic)<sub>3</sub>]<sup>2+</sup>, indicating a slower ligand exchange rate for [Ru<sup>II</sup>(tpy)(pic)<sub>3</sub>]<sup>2+</sup> and an essentially faster rate for [Ru<sup>II</sup>(pdc)(pic)<sub>3</sub>]<sup>2+</sup>.<sup>31,43</sup>

**Kinetics Study.** The formal rate constant (k<sub>cat</sub>) of the overall catalytic water oxidation (eq 10) was investigated by monitoring consumption of Ce<sup>IV</sup> in the presence of 1<sup>+</sup> under pH 1.0 conditions. In contrast to the O<sub>2</sub>-evolving experiments above, trials of evaluating k<sub>cat</sub> require a mild excess of Ce<sup>IV</sup>, typically tens of equivalents, in order to keep the absorbance decay of Ce<sup>IV</sup> consumption discernible over a reasonable period of time and conformable to the Beer–Lambert law. We chose 320 nm here as the characteristic wavelength to follow Ce<sup>IV</sup> consumption so as to avoid interference of a relatively strong absorption of 1<sup>+</sup> around 350 nm.



When the initial concentration of 1<sup>+</sup> was kept constant (0.025 mM) in the mixed solution and that of Ce<sup>IV</sup> changed

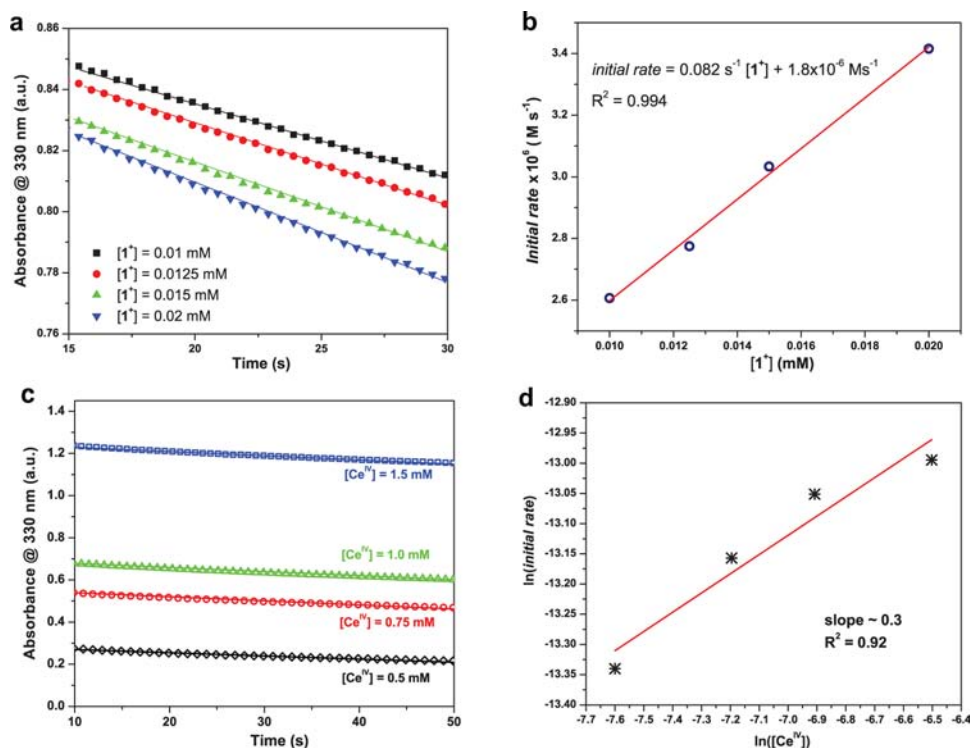


**Figure 6.** Kinetics and spectra data for  $Ce^{IV}$  consumption catalyzed by  $I^+$ . (a) Absorbance changes (330 nm) at various concentrations of  $I^+$ ; conditions initial  $[Ce^{IV}] = 1\ mM$ , pH 1.0  $HNO_3$ . (b) Initial rate of  $Ce^{IV}$  consumption versus concentration of  $I^+$ ; value of absorbance was transferred to the molarity of  $Ce^{IV}$  according to the Lambert–Beer law,  $\Delta C = \Delta A/\epsilon b$  (where  $\Delta C$  is the molarity change,  $\Delta A$  is the absorbance change,  $\epsilon$  is the molar extinction coefficient, and  $b$  is the path length of the cell). (c) Absorbance changes (330 nm) at various concentrations of  $Ce^{IV}$ ; conditions initial  $[I^+] = 0.025\ mM$ , pH 1.0  $HNO_3$ . (d) Natural logarithm of initial rate of  $Ce^{IV}$  consumption versus natural logarithm of concentration of  $Ce^{IV}$ .

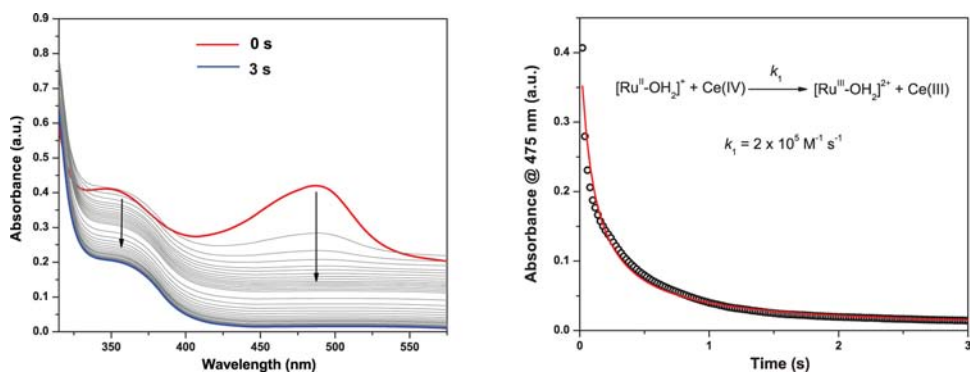


**Figure 7.** Kinetic and spectral data for oxidation of  $I^+$ . (Left) Spectral changes as a function of time after mixing  $I^+$  with 1 equiv of  $Ce^{IV}$ ; conditions  $[I^+] = 0.05\ mM$ , pH 1.0  $HNO_3$ . (Right) Fitting of absorbance change at 475 nm according to the reaction rate law.

(0.75–1.5 mM), the initial rate of  $Ce^{IV}$  consumption was partially dependent on  $[Ce^{IV}]$  (order < 1). The rate vs  $[Ce^{IV}]$  order was estimated to be ca. 0.3 by tracking the  $\ln(\text{rate})$  vs  $\ln([Ce^{IV}])$  slope (Figure 6c and 6d). The deviation of the  $\ln(\text{rate})/\ln([Ce^{IV}])$  relationship from linear is mainly because (i) the incipient segment (10 s) of the  $Ce^{IV}$  decay trace was not taken into account and (ii) at greater  $[Ce^{IV}]/[I^+]$  ratio the  $Ce^{IV}$ -involved rate-limiting step tends to flood others in the catalytic cycle. While the initial concentration of  $Ce^{IV}$  was kept constant (1 mM), the initial rate of  $Ce^{IV}$  consumption was found to be proportional to the initial concentration of  $I^+$  (0.01–0.02 mM, Figure 6a and 6b). Formally, the rate law of  $Ce^{IV}$  consumption can be expressed as initial rate =  $k[I^+][Ce^{IV}]^{0.3}$ . This evidence rationalized a dominant catalytic pathway that is first order in  $[I^+]$  and zero order in  $[Ce^{IV}]$ ,

following the rate expression initial rate =  $k_{\text{cat}} [I^+]$ . It also implies that there is an auxiliary path consuming  $Ce^{IV}$  simultaneously, and the rate of this concomitant process depends on  $[Ce^{IV}]$ . By neglecting the minor path, the formal rate constant of the dominant path  $k_{\text{cat}} = 0.02\ s^{-1}$  can be estimated as one-fourth of the initial rate of  $Ce^{IV}$  consumption versus  $[I^+]$  slope, because four  $Ce^{IV}$  cations were consumed in generation of each dioxygen. The realistic rate constant of the dominant path apparently should be smaller than  $0.02\ s^{-1}$ , which represents the combination of contributions from both major and minor paths of  $Ce^{IV}$  consumption.

Kinetics study on the consecutive ET steps of the catalytic cycle was carried out by successive addition of stoichiometric  $Ce^{IV}$  into a pH 1.0 solution of  $I^+$ . Mixing  $I^+$  with equimolar quantities of  $Ce^{IV}$  led to rapid oxidation of  $I^+$  to  $I^{2+}$

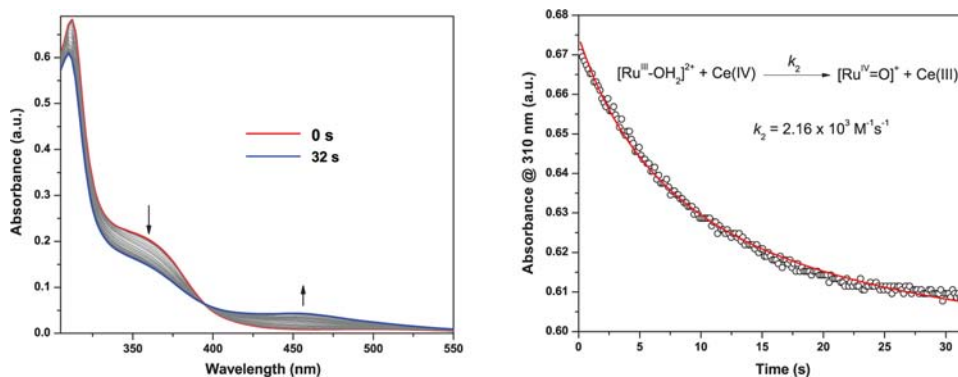


**Figure 8.** Kinetic and spectral data for oxidation of  $1^{2+}$ . (Left) Spectral changes as a function of time after mixing  $1^{2+}$  with 1 equiv of  $Ce^{IV}$ ; conditions  $[1^{2+}] = 0.05$  mM, pH 1.0  $HNO_3$ . (Right) Fitting of absorbance change at 310 nm according to the reaction rate law.

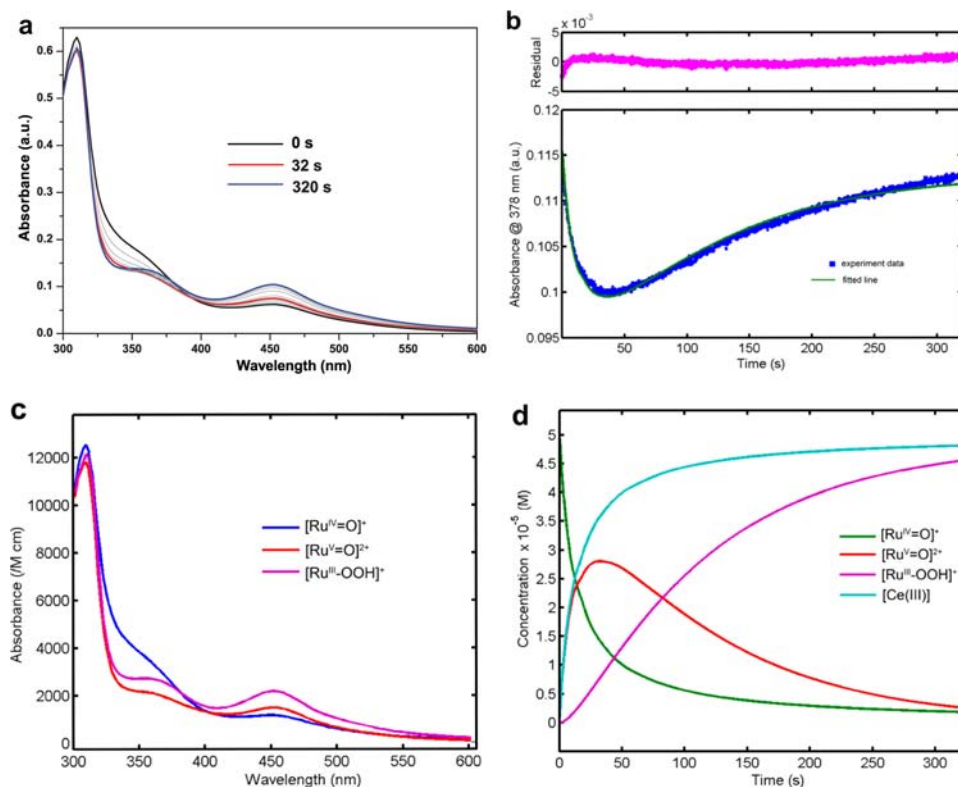
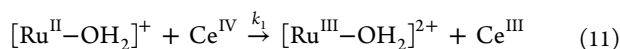


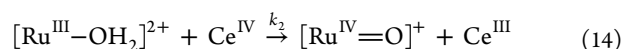
**Figure 9.** Kinetics and spectra data for generation of  $Ru^V$  species and formation of O–O bond. (a) Spectral changes as a function of time after mixing  $[Ru^{IV}(bpc)(bpy)O]^+$  with 1 equiv of  $Ce^{IV}$ ; conditions 0.05 mM complex in pH 1.0  $HNO_3$ . (b) Absorbance trace at 310 nm (blue dots) and fitting line (green). (c) Calculated absorption spectra for the ruthenium-containing species based on global fitting. (d) Diagram of species distribution versus time.

$([Ru^{III}(bpc)(bpy)OH_2]^{2+}$ , eq 11), of which a consequence is an immediate bleaching of MLCT bands of  $1^+$  at both 475 and 350 nm (Figure 7). This ET reaction is first order with regard to  $[1^+]$  as well as  $[Ce^{IV}]$ . The rate law of this step and its integrated expression are given in eqs 12 and 13, where  $A$ ,  $A_0$ , and  $A_\infty$  are absorbance at time  $t$ , 0, and infinity, respectively, and  $[Ru^{II}]_0$  is the initial concentration of  $1^+$ . The rate constant of this step  $k_1 = 2.0 \times 10^5 M^{-1} s^{-1}$  was determined by fitting the trace of absorbance decay at 475 nm according to the rate law in eq 13. Because this ET step was nearly accomplished in 3 s, the spectral profile at  $t = 3$  s is displayed in Figure 7 as a blue curve representing the absorbance spectrum of  $1^{2+}$ .



$$-\frac{d[Ru^{II}]}{dt} = k_1[Ru^{II}][Ce^{IV}] = k_1[Ru^{II}]^2 \quad (12)$$

$$\frac{(A_0 - A_\infty)}{[Ru^{II}]_0(A - A_\infty)} = k_1 t + \frac{1}{[Ru^{II}]_0} \quad (13)$$

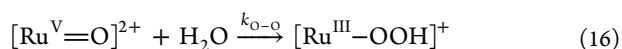
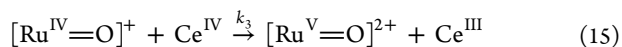


Addition of 1 equiv of  $Ce^{IV}$  to the pH 1.0  $HNO_3$  solution of  $1^{2+}$  generated the  $[Ru^{IV}=O]^+$  species (eq 14) through a PCET process, and a clear isosbestic point at 395 nm can be observed in the spectra vs time profiles (Figure 8). This  $Ru^{III} \rightarrow Ru^{IV}$  step has the same manner of reaction order as that of the previous  $Ru^{II} \rightarrow Ru^{III}$  step and thus follows the expressions of

rate law in eqs 12 and 13 too. The rate constant  $k_2 = 2.2 \times 10^3 \text{ M}^{-1} \text{ s}^{-1}$  was calculated by monitoring the absorbance decay at 310 nm. Compared with the  $\text{Ru}^{\text{II}} \rightarrow \text{Ru}^{\text{III}} \rightarrow \text{Ru}^{\text{IV}}$  oxidation sequence of  $[\text{Ru}^{\text{II}}(\text{tpy})(\text{bpy})\text{OH}_2]^{2+}$  under similar reaction conditions, of which the corresponding  $k_1$  and  $k_2$  were measured as  $4.4 \times 10^4$  and  $6.6 \times 10^3 \text{ M}^{-1} \text{ s}^{-1}$  respectively,<sup>15</sup> oxidation of  $\mathbf{1}^+$  to its  $\text{Ru}^{\text{III}}$  state is significantly faster, but the subsequent  $\text{Ru}^{\text{III}} \rightarrow \text{Ru}^{\text{IV}}$  step is considerably slower. This discovery substantiates the conclusion from our previous work that carboxylate groups can stabilize trivalent intermediates but restrict deprotonation of  $[\text{Ru}^{\text{III}}-\text{OH}_2]$  species.<sup>31</sup> We will discuss it with more detail in the following sections.

Meanwhile, the generated  $[\text{Ru}^{\text{IV}}=\text{O}]^+$  formation of  $\mathbf{1}^+$  was found unstable in pH 1.0  $\text{HNO}_3$ . After the incipient 40 s period of the  $\text{Ru}^{\text{III}} \rightarrow \text{Ru}^{\text{IV}}$  oxidation reaction, during which  $\mathbf{1}^{2+}$  in solution was almost depleted, a slow and slight recovery of the absorbance bands at 355 and 450 nm was observed in the time-resolved absorbance spectrum. We assume that the  $[\text{Ru}^{\text{IV}}=\text{O}]^+$  complex undergoes a slow disproportionation reaction, resulting in production of  $[\text{Ru}^{\text{III}}(\text{bpc})(\text{bpy})\text{OH}_2]^{2+}$  and  $[\text{Ru}^{\text{V}}(\text{bpc})(\text{bpy})\text{O}]^{2+}$  because the former  $\text{Ru}^{\text{III}}$  species features with moderate absorbance at 355 nm and the latter  $\text{Ru}^{\text{V}}$  species proceeds O–O bond formation triggering recovery of absorbance at 450 nm (vide infra). While further proof is desired to verify our assumption, a very similar instability of  $[\text{Ru}^{\text{IV}}(\text{tpy})(\text{bpy})\text{O}]^{2+}$  has been reported by Berlinguette et al. and attributed to a disproportionation decomposition.<sup>15</sup>

After addition of another 1 equiv of  $\text{Ce}^{\text{IV}}$  to the resulting  $[\text{Ru}^{\text{IV}}=\text{O}]^+$  formation of catalyst  $\mathbf{1}^+$ , a  $\text{Ru}^{\text{IV}} \rightarrow \text{Ru}^{\text{V}}$  ET step (eq 15) and a following water nucleophilic attack to the formally  $[\text{Ru}^{\text{V}}=\text{O}]^{2+}$  species (eq 16) can be rationalized by tracking the biphasic trace of time-resolved absorbance (Figure 9a and 9b). The rate law of this critical O–O bond formation step was described in eqs 17 and 18, where  $[\text{Ru}^{\text{V}}]$  is the concentration of  $[\text{Ru}^{\text{V}}=\text{O}]^{2+}$  species at time =  $t$  and  $k_{\text{O-O}}$  is the rate constant. Even though the  $[\text{Ru}^{\text{V}}=\text{O}]^{2+} \rightarrow [\text{Ru}^{\text{III}}-\text{OOH}]^+$  step was discerned obviously slower than the  $[\text{Ru}^{\text{IV}}=\text{O}]^+ \rightarrow [\text{Ru}^{\text{V}}=\text{O}]^{2+}$  step, these two processes did not completely separate during the initial period of reaction. Therefore, the observed absorbance spectra at certain time points were contributed by a combination of various species including tri-, tetra-, and pentavalent ruthenium complexes. A global fitting analysis (performed with ReactLab) based on the full spectral scheme (300–600 nm) and overall experimental time window (0–320 s) afforded rate constants as  $k_3 = 1.7 \times 10^3 \text{ M}^{-1} \text{ s}^{-1}$  and  $k_{\text{O-O}} = 1.1 \times 10^{-2} \text{ s}^{-1}$ . The calculated absorbance profiles of  $[\text{Ru}^{\text{IV}}=\text{O}]^{2+}$ ,  $[\text{Ru}^{\text{V}}=\text{O}]^{2+}$ , and  $[\text{Ru}^{\text{III}}-\text{OOH}]^+$  (Figure 9c) were in accordance with the observed spectral profiles at  $t = 0, 32$ , and 320 s, when corresponding species were shown to be predominant according to the calculated diagram of their time-dependent distribution (Figure 9d).



$$-\frac{d[\text{Ru}^{\text{V}}]}{dt} = k_{\text{O-O}}[\text{Ru}^{\text{V}}] \quad (17)$$

$$\ln\left(\frac{A - A_\infty}{A_0 - A_\infty}\right) = -k_{\text{O-O}}t \quad (18)$$

The values of  $k_3$  and  $k_{\text{O-O}}$  measured at different temperatures (10–25 °C, Table S2, Supporting Information) followed the Eyring equation (Figures S18 and S19, Supporting Information), from which the enthalpies and entropies of activation could be estimated (Table 2). At room temperature (293 K),

**Table 2. Activation Enthalpies and Entropies of Selected Steps in Catalytic Water Oxidation by  $\mathbf{1}^+$**

reactions	$\Delta H^\ddagger$ (kJ mol <sup>-1</sup> )	$\Delta S^\ddagger$ (J mol <sup>-1</sup> K <sup>-1</sup> )
$[\text{Ru}^{\text{IV}}=\text{O}] \rightarrow [\text{Ru}^{\text{V}}=\text{O}]$	$19.0 \pm 0.8$	$-113.7 \pm 4.0$
$[\text{Ru}^{\text{V}}=\text{O}] \rightarrow [\text{Ru}^{\text{III}}-\text{OOH}]$	$16.9 \pm 0.5$	$-196.6 \pm 12.5$

the Gibbs free energies of activation ( $\Delta G^\ddagger$ ) for  $[\text{Ru}^{\text{IV}}=\text{O}]^+ \rightarrow [\text{Ru}^{\text{V}}=\text{O}]^{2+}$  and  $[\text{Ru}^{\text{V}}=\text{O}]^{2+} \rightarrow [\text{Ru}^{\text{III}}-\text{OOH}]^+$  steps were calculated to be  $52.5 \pm 1.9$  and  $74.5 \pm 4.2$  kJ, respectively. It is not surprising that in the O–O bond formation step there is a quite large decrease of disorder from the reactants to the products, and entropy contributes significantly to the energy barrier.

All labeled rate constants of reactions involved in the catalytic cycle of water oxidation by  $\mathbf{1}^+$  are listed in Table 3. It

**Table 3. Rate Constants of  $\text{Ce}^{\text{IV}}$ -Driven Water Oxidation Catalyzed by  $\mathbf{1}^+$ , Measured at Room Temperature (20 °C) in pH 1.0  $\text{HNO}_3$**

rate constant (20 °C)	reaction description
$k_{\text{cat}} = 2 \times 10^{-2} \text{ s}^{-1}$	eq 10
$k_1 = 2.0 \times 10^5 \text{ M}^{-1} \text{ s}^{-1}$	eq 11
$k_2 = 2.2 \times 10^3 \text{ M}^{-1} \text{ s}^{-1}$	eq 14
$k_3 = 1.7 \times 10^3 \text{ M}^{-1} \text{ s}^{-1}$	eq 15
$k_{\text{O-O}} = 1.1 \times 10^{-2} \text{ s}^{-1}$	eq 16 (rate-determining step)

should be noted that they were measured at different conditions (different  $[\text{Ce}^{\text{IV}}]/[\mathbf{1}^+]$  ratios). With stoichiometric  $\text{Ce}^{\text{IV}}$ , the first oxidation process ( $k_1$  step) is extremely rapid and subsequent oxidation steps ( $k_2$  and  $k_3$  step) are slower but still much more rapid than the catalytic rate ( $k_{\text{cat}}$ ), and thereby none of these ET events represent the rate-determining step of the catalytic cycle. The rate constant ( $k_{\text{O-O}}$ ) of O–O bond formation is a little smaller than but close to  $k_{\text{cat}}$ . Taking into account that the overall catalytic reaction is nearly independent of the  $[\text{Ce}^{\text{IV}}]$  (during initial time), we conclude that O–O bond formation (eq 16) is the rate-determining step for water oxidation catalyzed by  $\mathbf{1}^+$ . Following steps might include oxidation of  $[\text{Ru}^{\text{III}}-\text{OOH}]^+$  to  $[\text{Ru}^{\text{IV}}-\text{OO}]^+$  or  $[\text{Ru}^{\text{V}}-\text{OO}]^{2+}$  species and liberation of  $\text{O}_2$  from the high-valent ruthenium core, as presumed by previous studies.<sup>15,20,21</sup> The stopped-flow method, however, is not applicable in these steps. The difference between  $k_{\text{cat}}$  and  $k_{\text{O-O}}$  reveals the presence of auxiliary pathways that consume  $\text{Ce}^{\text{IV}}$ . Concerned reactions include generation of  $\text{Ru}^{\text{VI}}$  species and O-atom transfer from  $\text{Ce}^{\text{IV}}$  hydroxide (or oxidation of ligand). These catalytic pathways of water oxidation by  $\mathbf{1}^+$  will be further discussed in the next section.

**Mass Spectrometric Study.** The ruthenium-containing species involved in the catalytic water oxidation by  $\mathbf{1}^+$  were inspected by mass spectrometry (MS). Both atmospheric-pressure chemical ionization (APCI) and electrospray ionization (ESI) sources were applied in this work. In a typical run,  $\mathbf{1}^+$  and  $\text{Ce}^{\text{IV}}$  were mixed in pH = 2.0  $\text{HNO}_3$  under furious stirring, and the resulting solution was immediately injected into MS

apparatus without any additional treatment. The reason for employing pH 2.0 solution instead of pH 1.0 solution is that the lighter ionic strength of the medium is helpful to trap charged species. In general, the typical isotopic distribution of ruthenium complexes makes their signals distinctive from other cation species, even though some MS peaks with very close  $m/z$  values can overlap with each other.

After addition of 1 equiv of  $\text{Ce}^{\text{IV}}$  in the pH 2.0 solution of  $1^+$ , the mass spectrum revealed a cluster at  $m/z = 474.0985$  (Figure 10, middle) as the only salient signal of Ru complexes, which

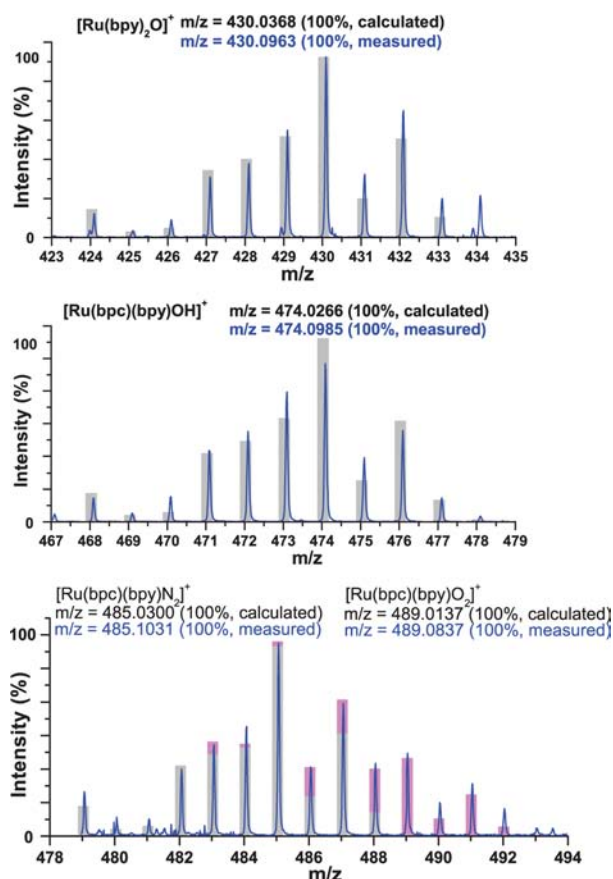


**Figure 10.** Observed and calculated mass spectra of assigned species after mixing  $1^+$  with 4–8 equiv of  $\text{Ce}^{\text{IV}}$  in pH = 2.0  $\text{HNO}_3$ . (Top)  $[\text{Ru}(\text{bpy})_2\text{O}]^+$ ; (middle)  $[\text{Ru}(\text{bpc})(\text{bpy})\text{OH}]^+$ ; (bottom) overlapped  $[\text{Ru}(\text{bpc})(\text{bpy})\text{N}_2]^+$  and  $[\text{Ru}(\text{bpc})(\text{bpy})\text{O}_2]^+$ , ideal spectrum was calculated with a ratio of  $[\text{Ru}(\text{bpc})(\text{bpy})\text{N}_2]^+$  (pink)/ $[\text{Ru}(\text{bpc})(\text{bpy})\text{O}_2]^+$  (gray) = 3/1.

could be assigned to  $[\text{Ru}^{\text{III}}(\text{bpc})(\text{bpy})\text{OH}]^+$ . Addition of another 3 equiv of  $\text{Ce}^{\text{IV}}$  led to the emergence of two clusters of Ru-containing species in the MS spectrum at around  $m/z = 430.0963$  and  $485.1031$ , respectively, of which the intensity is relatively weak, about 10% of the mass spectrum. The former signal (Figure 10, top) corresponds to  $[\text{Ru}(\text{bpy})_2\text{O}]^+$ , which might be converted from  $\text{Ru}^{\text{IV}}\text{-oxo}$  or  $\text{Ru}^{\text{V}}\text{-oxo}$  species by loss of one  $\text{CO}_2$ . This kind of Ru-catalyzed decarboxylation is known as a highly endothermic process,<sup>44</sup> and cleavage of the benzyl-carboxylate bond can be mediated by either  $\text{Ru}^{\text{IV}}$  or  $\text{Ru}^{\text{V}}$  complexes.<sup>45</sup> This decarboxylation disclosed a decomposition manner of  $1^+$  under  $\text{Ce}^{\text{IV}}$ -driven water oxidation conditions.

The latter cluster (Figure 10, bottom) was assigned as overlapped signals of  $[\text{Ru}(\text{bpc})(\text{bpy})\text{N}_2]^+$  and  $[\text{Ru}(\text{bpc})(\text{bpy})\text{-}$

$\text{O}_2]^+$ . While the existence of  $[\text{Ru}^{\text{IV}}(\text{bpc})(\text{bpy})\text{O}_2]^+$  from oxidation of  $[\text{Ru}^{\text{III}}(\text{bpc})(\text{bpy})\text{-OOH}]^+$  has been presumed by another study as well as ours here, discovery of  $[\text{Ru}(\text{bpc})(\text{bpy})\text{N}_2]^+$  is a little unexpected. We infer that  $\text{N}_2$  bonds with the Ru center after release of  $\text{O}_2$  from  $[\text{Ru}^{\text{IV}}(\text{bpc})(\text{bpy})\text{O}_2]^+$ . Although dinitrogen is generally regarded inert and reluctant to coordinate with transition metals, displacement of other ligands by  $\text{N}_2$  and formation of the Ru– $\text{N}_2$  bond have been reported before.<sup>46</sup> Generation of  $[\text{Ru}(\text{bpc})(\text{bpy})\text{N}_2]^+$  might be favored by the intensive  $\text{N}_2$  atmosphere under MS experimental conditions. A similar  $[\text{Ru}\text{-N}_2]^+$  species was also detected by Sakai et al. during their study on  $[\text{Ru}^{\text{II}}(\text{tpy})(\text{bpy})\text{OH}_2]^{2+}$ .<sup>13</sup> Adding more  $\text{Ce}^{\text{IV}}$  (8 equiv in all) did not lead to exposure of any other ruthenium species but enhancement of the signals at  $m/z = 430.0963$  and  $485.1031$ . It should be noted that the environment within MS apparatus is quite different from that of aqueous solutions. A strong MS signal does not necessarily indicate a high concentration of corresponding species in solutions. A dominant species in solution, vice versa, might be too fragile to be trapped under MS experimental conditions.

Additionally, the mass spectrum of  $[\text{Ru}^{\text{III}}(\text{bpc})(\text{pic})_2\text{OH}]^+$  could be recorded after mixing  $2^+$  with 1–4 equiv of  $\text{Ce}^{\text{IV}}$  in pH 2.0  $\text{HNO}_3$  (Figure S20, Supporting Information). The  $[\text{Ru}^{\text{III}}(\text{bpc})(\text{pic})_2\text{OH}_2]^{2+}$  species was generated via replacement of one picoline of  $[\text{Ru}^{\text{III}}(\text{bpc})(\text{pic})_3]^+$  by water. Under MS experimental conditions, the aqua– $\text{Ru}^{\text{III}}$  complex seems to be prone to reduce its positive charge by losing one of its protons. The mass signal of  $[\text{Ru}^{\text{III}}(\text{bpc})(\text{pic})_2\text{OH}]^+$  herein should originate from the corresponding aqua– $\text{Ru}^{\text{III}}$  complex in solution.

## DISCUSSION

On the basis of the experimental results addressed above, we proposed a catalytic cycle of water oxidation by  $1^+$  as drawn in Figure 11. The critical step is O–O bond formation through a

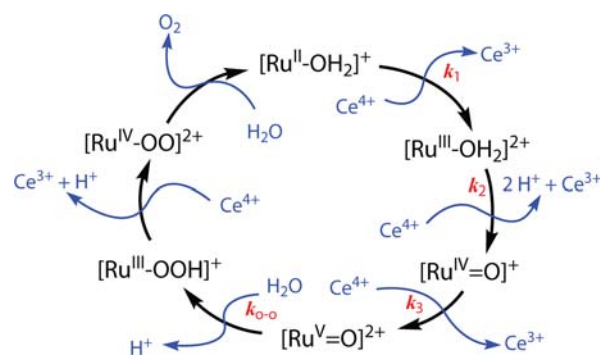


**Figure 11.** Proposed catalytic cycle of water oxidation (dominant) catalyzed by  $1^+$ .

water nucleophilic attack (also called ‘acid–base’ mechanism, which was first established for  $[\text{Ru}^{\text{II}}(\text{tpy})(\text{bpm})\text{OH}_2]^{2+}$  by Meyer et al.<sup>20</sup> and then expanded to other  $[\text{Ru}(\text{N}_3)(\text{N}_2)\text{L}]$  type of WOCs, such as  $[\text{Ru}^{\text{II}}(\text{tpy})(\text{bpy})\text{OH}_2]^{2+}$  derivatives.<sup>15</sup> Despite the similar mechanism scenario and coordination geometry between  $1^+$  and  $[\text{Ru}(\text{N}_3)(\text{N}_2)\text{L}]$  WOCs, especially  $[\text{Ru}^{\text{II}}(\text{tpy})(\text{bpy})\text{OH}_2]^{2+}$ , we found that introduction of anionic tridentate bpc ligand almost influences every individual step included in the catalytic cycle in comparison with neutral tridentate tpy ligand. The major topic in this Discussion section

is a close look at these disparities in order to understand the ligand role with respect to catalytic water oxidation.

In pH 1.0 medium, the  $[\text{Ru}^{\text{II}}-\text{OH}_2]^+ \rightarrow [\text{Ru}^{\text{III}}-\text{OH}_2]^{2+}$  step of  $\mathbf{1}^+$  happens in a faster rate ( $k_1 = 2.0 \times 10^5 \text{ M}^{-1} \text{ s}^{-1}$ ) and at a lower potential ( $E^{1/2}(\text{Ru}^{\text{III}}/\text{Ru}^{\text{II}}) = 0.81 \text{ V}$  vs NHE) than that of  $[\text{Ru}^{\text{II}}(\text{tpy})(\text{bpy})\text{OH}_2]^{2+}$  or  $[\text{Ru}^{\text{II}}(\text{tpy})(\text{bpm})\text{OH}_2]^{2+}$ ; <sup>20,43,47</sup> the subsequent  $[\text{Ru}^{\text{III}}-\text{OH}_2]^{2+} \rightarrow [\text{Ru}^{\text{IV}}=\text{O}]^+$  step of  $\mathbf{1}^+$  is at a similar rate ( $k_2 = 2.2 \times 10^3 \text{ M}^{-1} \text{ s}^{-1}$ ) and potential of the same level ( $E^{1/2}(\text{Ru}^{\text{IV}}/\text{Ru}^{\text{III}}) = 1.29 \text{ V}$ ) compared to that of the referred two complexes; the further  $[\text{Ru}^{\text{IV}}=\text{O}]^+ \rightarrow [\text{Ru}^{\text{V}}=\text{O}]^{2+}$  step of  $\mathbf{1}^+$  is again faster ( $k_3 = 1.7 \times 10^3 \text{ M}^{-1} \text{ s}^{-1}$ ) and more facile ( $E^{1/2}(\text{Ru}^{\text{V}}/\text{Ru}^{\text{IV}}) = 1.57 \text{ V}$ ). The reason is that the carboxylate group can donate a lone pair to the high-valent Ru center via  $p\pi-d\pi$  interaction and increase its electron density accordingly. This benefits extraction of electrons from the Ru core but compromises release of protons from the complex. As a consequence, we see the positive effect of bpc ligand upon ET steps but not PCET process compared to neutral tridentate ligands, like tpy. The  $\text{p}K_{\text{a}}$  values of  $\mathbf{1}^+$  and  $\mathbf{1}^{2+}$  are 10.6 and 2.6, respectively, higher than those of  $[\text{Ru}^{\text{II}}(\text{tpy})(\text{bpy})\text{OH}_2]^{2+}$  ( $\text{p}K_{\text{a}} = 9.7$ ) and  $[\text{Ru}^{\text{III}}(\text{tpy})(\text{bpy})\text{OH}_2]^{3+}$  ( $\text{p}K_{\text{a}} = 1.7$ ).<sup>47</sup> It is evident that  $\mathbf{1}^+$  and  $\mathbf{1}^{2+}$  are more reluctant to liberate protons. The potential separation between the  $\text{Ru}^{\text{III}}/\text{Ru}^{\text{II}}$  and the  $\text{Ru}^{\text{IV}}/\text{Ru}^{\text{III}}$  redox couples of  $\mathbf{1}^+$  is approximately 300 mV over the pH range of 2.6–10.6.

Basically, the higher electron density of metal center is aligned with the lower electrophilicity of the  $[\text{Ru}^{\text{V}}=\text{O}]$  fragment. The observed water nucleophilic attack to  $[\text{Ru}^{\text{V}}(\text{bpc})(\text{bpy})=\text{O}]^{2+}$  ( $k_{\text{O}-\text{O}} = 1.1 \times 10^{-2} \text{ s}^{-1}$ ) is, however, not slower than that to  $[\text{Ru}^{\text{V}}(\text{tpy})(\text{bpm})=\text{O}]^{3+}$  ( $k_{\text{O}-\text{O}} = 0.96 \times 10^{-2} \text{ s}^{-1}$ ). The disadvantage of electrophilic factors in the case of  $\text{Ru}^{\text{V}}-\text{bpc}$  species might be compensated by association of protons within the reaction and the assistance of hydrogen bonding between the carbonyl group and the incoming water. This O–O bond formation step is regarded as the rate-determining step of the catalytic cycle because (i)  $k_{\text{O}-\text{O}}$  is smaller but comparable with regard to the formal catalytic rate constant  $k_{\text{cat}}$ , (ii) the initial rate of  $\text{Ce}^{\text{IV}}$  consumption is nearly irrelevant to the concentration of  $\text{Ce}^{\text{IV}}$  (0.3 order) under catalytic conditions, and (iii) the onset of catalytic current and the  $\text{Ru}^{\text{V}}/\text{Ru}^{\text{IV}}$  redox event are concomitant in potential sweep measurements. The  $[\text{Ru}(\text{bpy})_2\text{O}]^+$  species recorded in the MS experiment tentatively derives from the  $[\text{Ru}^{\text{V}}(\text{bpc})(\text{bpy})=\text{O}]^{2+}$  intermediate. This decarboxylation process ( $\text{bpc} \rightarrow \text{bpy}$ ) itself can be mediated by pentavalent ruthenium and tremendously magnified under MS experimental conditions, because the reaction is highly endothermic and the temperature of the ionization source within mass spectrometry is very high (180 °C). The same degradation reaction could happen in aqueous solution under water oxidation conditions, but it is hard to estimate the extent.

The subsequent  $[\text{Ru}^{\text{III}}-\text{OOH}]^+ \rightarrow [\text{Ru}^{\text{IV}}-\text{OO}]^+$  step cannot be probed by stopped-flow method, but it is believed to be rapid. Formation of  $[\text{Ru}^{\text{IV}}(\text{bpc})(\text{bpy})\text{O}_2]^+$  was corroborated by the mass spectrum. Dissociation of  $\text{O}_2$  from  $[\text{Ru}^{\text{IV}}-\text{OO}]^+$  species was believed to be the rate-determining step for those  $[\text{Ru}(\text{N}_3)(\text{N}_2)\text{L}]$  types of WOCs carrying only polypyridyl ligands.<sup>15,21</sup> In contrast, it is not the case for  $\mathbf{1}^+$ . Even though the rate constant of the step was not measured directly, it should be no smaller than  $k_{\text{O}-\text{O}} = 1.1 \times 10^{-2} \text{ s}^{-1}$ . Facile release of  $\text{O}_2$  from  $[\text{Ru}^{\text{IV}}(\text{bpc})(\text{bpy})\text{O}_2]^+$  can be interpreted by the stabilization effect of the carboxylate group upon the high-valent Ru center, e.g.,  $p(\pi)$ -donating ability of carboxylate

donor to the electron-deficient ruthenium center stabilizes the coordinatively unsaturated intermediate. The same stabilization effect was also applied to the labile picoline ligand of  $\mathbf{2}^{2+}$  as well as other complexes with carboxylate ligand we reported before.<sup>31</sup> This effect is more significant in neutral conditions rather than acidic conditions because protonation of the carbonyl group attenuates the electron-donating ability of the carboxylate donor. Considering easier access of the  $[\text{Ru}^{\text{V}}=\text{O}]$  state for  $\mathbf{1}^+$  relative to other  $[\text{Ru}(\text{N}_3)(\text{N}_2)\text{L}]$  type of complexes, we cannot rule out the possibility of further oxidation of  $[\text{Ru}^{\text{IV}}(\text{bpc})(\text{bpy})\text{O}_2]^+$  to  $[\text{Ru}^{\text{V}}(\text{bpc})(\text{bpy})\text{O}_2]^{2+}$  in pH 1.0  $\text{Ce}^{\text{IV}}$  solution, although this oxidation reaction is merely applicable in pH 0/ $\text{Ce}^{\text{IV}}$  solution for most  $[\text{Ru}(\text{N}_3)(\text{N}_2)\text{L}]$  WOCs. Theoretical studies are underway about the divergent feasible paths after generation of  $[\text{Ru}^{\text{IV}}-\text{OO}]^+$  species.

Other findings in the study disclosed more complications in the realistic water oxidation reaction catalyzed by  $\mathbf{1}^+$ . The rate constant of  $\text{O}_2$  evolution for  $\mathbf{1}^+$  ( $k_{\text{O}_2} = 0.165 \text{ s}^{-1}$ ) is about eight times larger than  $k_{\text{cat}}$  ( $2 \times 10^{-2} \text{ s}^{-1}$ ). If the ‘acid–base’ catalytic pathway is dominant, no matter what the concentration of  $\text{Ce}^{\text{IV}}$  is,  $k_{\text{O}_2}$  would be equal to one-fourth of the value of  $k_{\text{cat}}$ . Thus, there must be an ‘ancillary’ (or prevailing) water oxidation pathway that overwhelms the ‘acid–base’ pathway discussed above, when a large excess of  $\text{Ce}^{\text{IV}}$  is present (circumstance in the measurement of  $k_{\text{O}_2}$ ). Certainly, this ‘ancillary’ pathway should bypass the step of water nucleophilic attack to  $[\text{Ru}^{\text{V}}=\text{O}]^{2+}$  species, of which the rate constant is determined and irrelevant to  $[\text{Ce}^{\text{IV}}]$ . Taking the following facts into account, initial rate of  $\text{O}_2$  evolution is first order in  $[\mathbf{1}^+]$  and a large excess  $[\text{Ce}^{\text{IV}}]$  dramatically enhances the rate of the catalytic reaction, we conclude that the rate of the ‘ancillary’ water oxidation pathway is first order in the concentration of catalyst and depends on the concentration of  $\text{Ce}^{\text{IV}}$ .

Additionally, we noted that (i)  $k_{\text{cat}}$  is larger (about twice) than  $k_{\text{O}-\text{O}}$  and (ii) the rate of  $\text{Ce}^{\text{IV}}$  consumption is slightly related to the concentration of  $\text{Ce}^{\text{IV}}$  (in the circumstance of mildly excess  $[\text{Ce}^{\text{IV}}]$ ), deviating from a straight rate/time line. Both experimental observations are reasonable if the ‘ancillary’ pathway depending on  $[\text{Ce}^{\text{IV}}]$  is concerned. On one hand,  $k_{\text{cat}}$  was measured in the presence of tens of equivalents of  $\text{Ce}^{\text{IV}}$ , and thus, the observed initial rate of  $\text{Ce}^{\text{IV}}$  consumption was ascribed to reactions of the combined water nucleophilic attack and ‘ancillary’ pathways, namely, the  $\text{Ce}^{\text{IV}}$  consumption rate via the water nucleophilic attack pathway is overestimated if the ‘ancillary’ pathway is taken into account. On the other hand, the rate of  $\text{Ce}^{\text{IV}}$  consumption is susceptible to the concentration of  $\text{Ce}^{\text{IV}}$  and decreases as  $\text{Ce}^{\text{IV}}$  is constantly being depleted over time. Thus, the overall  $\text{Ce}^{\text{IV}}$  consumption rate is dwindling as the reaction proceeds. (During the initial time, the change of  $[\text{Ce}^{\text{IV}}]$  is trivial in each trial of experiment and can be neglected.) In fact, the  $\text{Ce}^{\text{IV}}$  consumption rates during the reaction time of 300–400 s still depends linearly on the concentration of  $\mathbf{1}^+$  (Figure S21, Supporting Information), when the ‘ancillary’ pathway is much less notable than that at the initial time (15–30 s). In this situation, the measured catalytic rate ( $k_{\text{cat}}' = 0.81 \times 10^{-2} \text{ s}^{-1}$ ) is a little smaller than  $k_{\text{O}-\text{O}}$ . The decrement from  $k_{\text{cat}}$  to  $k_{\text{cat}}'$  is due to exclusion of the ‘ancillary’ catalytic pathway and inclusion of considerable catalyst decomposition.

## CONCLUSIONS

Two novel mononuclear ruthenium complexes ( $\mathbf{1}^+\text{PF}_6^-$  and  $\mathbf{2}^+\text{PF}_6^-$ ) containing an anionic ligand were prepared and

explicitly characterized. Both of them were studied for catalytic water oxidation in acidic (pH 1.0)  $\text{Ce}^{\text{IV}}$  medium. Kinetics study based on aqua complex  $\text{I}^+$  revealed that under stoichiometric  $\text{Ce}^{\text{IV}}$  conditions O–O bond formation by water nucleophilic attack to the  $[\text{Ru}^{\text{V}}=\text{O}]^{2+}$  formation of  $\text{I}^+$  is the rate-determining step. By comparing with representative  $[\text{Ru}(\text{N}_3)(\text{N}_2)\text{L}]$  kind of WOCs, namely,  $[\text{Ru}^{\text{II}}(\text{tpy})(\text{bpy})\text{OH}_2]^{2+}$  and  $[\text{Ru}^{\text{II}}(\text{tpy})(\text{bpm})\text{OH}_2]^{2+}$ , our study provides insight on how inherent properties of the carboxylate ligand influence the catalytic cycle ('acid–base') of water oxidation by monomeric Ru complexes. The advantages of introduction of carboxylate donor include (i) reducing the redox potential of accessing high-valent ( $\text{Ru}^{\text{IV}}$  and  $\text{Ru}^{\text{V}}$ , for example) states of ruthenium WOCs, (ii) reducing the overpotential of catalytic water oxidation, (iii) enhancing the rate of ligand exchange ( $\text{H}_2\text{O}/\text{pic}$  in this case), (iv) facilitating release of dioxygen from the ruthenium center, and (v) possibly drawing the water molecule close to the reactive Ru site via a hydrogen bond. Disadvantages include retardation of proton transfer and potential ways of degradation (such as decarboxylation and ligand dissociation).

In the presence of a large excess of  $\text{Ce}^{\text{IV}}$  (thousands of equivalents), however, experimental evidence implied an 'ancillary' water oxidation pathway overwhelming the water nucleophilic attack pathway. This 'ancillary' pathway is discernible but not obvious under the condition of a mild excess  $\text{Ce}^{\text{IV}}$  (tens of equivalents). While it is clear that the rate of the 'ancillary' water oxidation pathway is related to the concentration of  $\text{Ce}^{\text{IV}}$ , there is a lack of concrete evidence to delineate a vivid plot of the 'ancillary' pathway now.

## ■ ASSOCIATED CONTENT

### ■ Supporting Information

CIF files, selected crystal data, further NMR (1D and 2D) details, supplementary spectral figures for the reported complexes, and additional experimental information in the kinetics and thermodynamics study. This material is available free of charge via the Internet at <http://pubs.acs.org>.

## ■ AUTHOR INFORMATION

### ■ Corresponding Author

\*Phone: +46-8-7908127. Fax: +46-8-7912333. E-mail: [lichengs@kth.se](mailto:lichengs@kth.se).

### ■ Notes

The authors declare no competing financial interest.

## ■ ACKNOWLEDGMENTS

We thank the Swedish Research Council (VR), the Swedish Governmental Agency for Innovation Systems (VINNOVA), the K&A Wallenberg Foundation, the Swedish Energy Agency, the China Scholarship Council, the National Science Foundation of China (Grants 21120102036 and 20923006), and the National Basic Research Program of China (Grant 2009CB220009) for financial support of this work. We thank Björn Åkermark and his colleagues at Stockholm University for their help with MS measurement.

## ■ REFERENCES

- (1) Barber, J. *Chem. Soc. Rev.* **2009**, *38*, 185.
- (2) Dau, H.; Zaharieva, I. *Acc. Chem. Res.* **2009**, *42*, 1861.
- (3) Umena, Y.; Kawakami, K.; Shen, J.-R.; Kamiya, N. *Nature* **2011**, *473*, 55.
- (4) Lewis, N. S.; Nocera, D. G. *Proc. Natl. Acad. Sci. U.S.A.* **2006**, *103*, 15729.

- (5) Sala, X.; Romero, I.; Rodríguez, M.; Escriche, L.; Llobet, A. *Angew. Chem., Int. Ed.* **2009**, *48*, 2842.
- (6) Duan, L.; Tong, L.; Xu, Y.; Sun, L. *Energy Environ. Sci.* **2011**, *4*, 3296.
- (7) Dau, H.; Limberg, C.; Reier, T.; Risch, M.; Roggan, S.; Strasser, P. *ChemCatChem* **2010**, *2*, 724.
- (8) Artero, V.; Chavarot-Kerlidou, M.; Fontecave, M. *Angew. Chem., Int. Ed.* **2011**, *50*, 7238.
- (9) Concepcion, J. J.; Jurss, J. W.; Brennaman, M. K.; Hoertz, P. G.; Patrocinio, A. O. T.; Murakami Iha, N. Y.; Templeton, J. L.; Meyer, T. J. *Acc. Chem. Res.* **2009**, *42*, 1954.
- (10) Concepcion, J. J.; Jurss, J. W.; Norris, M. R.; Chen, Z.; Templeton, J. L.; Meyer, T. J. *Inorg. Chem.* **2010**, *49*, 1277.
- (11) Kaveevivitchai, N.; Zong, R.; Tseng, H.-W.; Chitta, R.; Thummel, R. P. *Inorg. Chem.* **2012**, *51*, 2930.
- (12) Tseng, H.-W.; Zong, R.; Muckerman, J. T.; Thummel, R. *Inorg. Chem.* **2008**, *47*, 11763.
- (13) Masaoka, S.; Sakai, K. *Chem. Lett.* **2009**, *38*, 182.
- (14) Yoshida, M.; Masaoka, S.; Abe, J.; Sakai, K. *Chem. Asian J.* **2010**, *5*, 2369.
- (15) Wasylenko, D. J.; Ganesamoorthy, C.; Henderson, M. A.; Koivisto, B. D.; Osthoff, H. D.; Berlinguette, C. P. *J. Am. Chem. Soc.* **2010**, *132*, 16094.
- (16) Wasylenko, D. J.; Ganesamoorthy, C.; Koivisto, B. D.; Henderson, M. A.; Berlinguette, C. P. *Inorg. Chem.* **2010**, *49*, 2202.
- (17) Yamazaki, H.; Hakamata, T.; Komi, M.; Yagi, M. *J. Am. Chem. Soc.* **2011**, *133*, 8846.
- (18) Boyer, J. L.; Polyansky, D. E.; Szalda, D. J.; Zong, R.; Thummel, R. P.; Fujita, E. *Angew. Chem., Int. Ed.* **2011**, *50*, 12600.
- (19) Romain, S.; Vigara, L.; Llobet, A. *Acc. Chem. Res.* **2009**, *42*, 1944.
- (20) Concepcion, J. J.; Jurss, J. W.; Templeton, J. L.; Meyer, T. J. *J. Am. Chem. Soc.* **2008**, *130*, 16462.
- (21) Concepcion, J. J.; Tsai, M.-K.; Muckerman, J. T.; Meyer, T. J. *J. Am. Chem. Soc.* **2010**, *132*, 1545.
- (22) Sala, X.; Ertem, M. Z.; Vigara, L.; Todorova, T. K.; Chen, W.; Rocha, R. C.; Aquilante, F.; Cramer, C. J.; Gagliardi, L.; Llobet, A. *Angew. Chem., Int. Ed.* **2010**, *49*, 7745.
- (23) Polyansky, D. E.; Muckerman, J. T.; Rochford, J.; Zong, R.; Thummel, R. P.; Fujita, E. *J. Am. Chem. Soc.* **2011**, *133*, 14649.
- (24) Tong, L.; Duan, L.; Xu, Y.; Privalov, T.; Sun, L. *Angew. Chem., Int. Ed.* **2010**, *50*, 445.
- (25) Duan, L.; Fischer, A.; Xu, Y.; Sun, L. *J. Am. Chem. Soc.* **2009**, *131*, 10397.
- (26) Xu, Y.; Åkermark, T.; Gyollai, V.; Zou, D.; Eriksson, L.; Duan, L.; Zhang, R.; Åkermark, B.; Sun, L. *Inorg. Chem.* **2009**, *48*, 2717.
- (27) Xu, Y.; Fischer, A.; Duan, L.; Tong, L.; Gabrielsson, E.; Åkermark, B.; Sun, L. *Angew. Chem., Int. Ed.* **2010**, *49*, 8934.
- (28) Duan, L.; Xu, Y.; Gorlov, M.; Tong, L.; Andersson, S.; Sun, L. *Chem.—Eur. J.* **2010**, *16*, 4659.
- (29) Duan, L.; Xu, Y.; Zhang, P.; Wang, M.; Sun, L. *Inorg. Chem.* **2010**, *49*, 209.
- (30) Duan, L.; Bozoglian, F.; Mandal, S.; Stewart, B.; Privalov, T.; Llobet, A.; Sun, L. *Nat Chem* **2012**, *4*, 418.
- (31) Tong, L.; Wang, Y.; Duan, L.; Xu, Y.; Cheng, X.; Fischer, A.; Ahlquist, M. S. G.; Sun, L. *Inorg. Chem.* **2012**, *51*, 3388.
- (32) Kimoto, A.; Yamauchi, K.; Yoshida, M.; Masaoka, S.; Sakai, K. *Chem. Commun.* **2012**, *48*, 239.
- (33) Garber, T.; Van Wallendael, S.; Rillema, D. P.; Kirk, M.; Hatfield, W. E.; Welch, J. H.; Singh, P. *Inorg. Chem.* **1990**, *29*, 2863.
- (34) Toyama, M.; Inoue, K.-i.; Iwamatsu, S.; Nagao, N. *Bull. Chem. Soc. Jpn.* **2006**, *79*, 1525.
- (35) Sheldrick, G. *Acta Crystallogr., Sect. A* **2008**, *64*, 112.
- (36) Spiccia, L.; Deacon, G. B.; Kepert, C. M. *Coord. Chem. Rev.* **2004**, *248*, 1329.
- (37) Yang, X.-J.; Drepper, F.; Wu, B.; Sun, W.-H.; Haehnel, W.; Janiak, C. *Dalton Trans.* **2005**, 256.
- (38) Nyhlen, J.; Duan, L.; Åkermark, B.; Sun, L.; Privalov, T. *Angew. Chem., Int. Ed.* **2010**, *49*, 1773.

- (39) Privalov, T.; Åkermark, B.; Sun, L. *Chem.—Eur. J.* **2011**, *17*, 8313.
- (40) Chen, Z.; Concepcion, J. J.; Luo, H.; Hull, J. F.; Paul, A.; Meyer, T. J. *J. Am. Chem. Soc.* **2010**, *132*, 17670.
- (41) Hartwig, J. F. *Organotransition Metal Chemistry: From Bonding to Catalysis*; University Science Books: Mill Valley, CA, 2009.
- (42) Yagi, M.; Tajima, S.; Komi, M.; Yamazaki, H. *Dalton Trans.* **2011**, *40*, 3802.
- (43) Duan, L.; Xu, Y.; Tong, L.; Sun, L. *ChemSusChem* **2011**, *4*, 238.
- (44) Gooßen, L. J.; Rodríguez, N.; Gooßen, K. *Angew. Chem., Int. Ed.* **2008**, *47*, 3100.
- (45) Chatani, N.; Tatamidani, H.; Ie, Y.; Kakiuchi, F.; Murai, S. *J. Am. Chem. Soc.* **2001**, *123*, 4849.
- (46) MacKay, B. A.; Fryzuk, M. D. *Chem. Rev.* **2004**, *104*, 385.
- (47) Takeuchi, K. J.; Thompson, M. S.; Pipes, D. W.; Meyer, T. J. *Inorg. Chem.* **1984**, *23*, 1845.